Table VIII. Highest Occupied Molecular Orbital (HOMO) Levels, in eV

	PH_n	AsH_n	PCl_n
AX_3	−10.38	−10.16	−11.63 (−11.21)[a]
AX_4^+	−22.78	−21.68	−19.17
AX_4^-	−1.27	1.56	−5.78
AX_5	−8.84	−8.58	−12.66
AX_6^-	−2.98	−3.17	−8.02

[a] With d functions on chlorine.

of eigenvalues for all species studied here are available upon request. They show an expected upward shift of the levels from PH_n to AsH_n, except for the HOMO levels of AsH_4^- and AsH_6^-. Nevertheless, this shift is small. We give in Table VIII the HOMO levels, which can be related to the first ionization potentials through Koopmans' theorem.

From a structural point of view, an ion such as PCl_5^{2-} (which is not known, but SbF_5^{2-} and $SbCl_5^{2-}$ are known) can be related to PCl_6^- since both have 6 electron pairs around the phosphorus atom. Consequently one can predict for PCl_5^{2-} a C_{4v} structure with an angle $\angle(r_{basal},r_{apical}) < 90°$. The situation of PCl_6^{3-} is different[58] since this ion possesses a seventh lone pair that may or may not be stereochemically active, giving a fluxional, near-octahedron like XeF_6 or a rigid octahedron like $TeCl_6^{2-}$.

In conclusion, the main results of our calculations are the following: (1) pentacoordinate phosphorus and arsenic compounds have a Lewis acid character; (2) hexacoordinate PX_6^- species have a rigid structure,[59] unlike PX_5 species; (3) their isomerization occurs preferably through bond rupture via a pentacoordinate intermediate; (4) structures of phosphorus and arsenic compounds are similar and so are the barriers to pseudorotation in PH_5 and AsH_5; and (5) some energetic differences between phosphorus and arsenic multicoordinate compounds are significant, for instance the tendency toward a greater stability for arsoranides.

Acknowledgment. We are indebted to Drs. A. Klaebe, M. Koenig, and J. G. Wolf for many discussions and comments and to the referees for helpful criticisms.

Registry No. PH_3, 7803-51-2; AsH_3, 7784-42-1; PCl_3, 7719-12-2; PH_4^+, 16749-13-6; AsH_4^+, 53250-40-1; PCl_4^+, 15169-50-3; PH_4^-, 20774-06-5; AsH_4^-, 90858-36-9; PCl_4^-, 29962-22-9; PH_5, 13769-19-2; AsH_5, 16612-59-2; PCl_5, 10026-13-8; PH_6^-, 79839-88-6; AsH_6^-, 90858-37-0; PCl_6^-, 16920-87-9; P, 7723-14-0; As, 7440-38-2; H^+, 12408-02-5; H^-, 12184-88-2; H_2, 1333-74-0; Cl_2, 7782-50-5; Cl^-, 16887-00-6.

(57) In PH_3 and AsH_3, we have the ratio $(k_{PH}/k_{AsH})^{1/2} = 1.09$ which is, incidentally, the ratio of the corresponding stretching frequencies (McKean, D. C.; Torio, I.; Morrisson, A. R. *J. Phys. Chem.* **1982**, *86*, 307), but the latter may follow directly from the atomic masses involved.

(58) An observation of PCl_6^{3-} has been reported: Nabi, S. N.; Hussain, A.; Ahmed, N. N. *J. Chem. Soc., Dalton Trans.* **1974**, 1199.

(59) At least when X = H or Cl. Recently, fluxional PX_6^- species containing three or more fluorine atoms have been reported: Dillon, K. B.; Platt, A. W. G. *J. Chem. Soc., Chem. Commun.* **1983**, *19*, 1089.

Deoxygenation of a Cluster-Coordinated Nitric Oxide

Douglas E. Fjare and Wayne L. Gladfelter*[1]

Department of Chemistry, The University of Minnesota, Minneapolis, Minnesota 55455.
Received January 9, 1984

Abstract: The reaction of $[Fe(CO)_3(NO)]^-$ with $Ru_3(CO)_{12}$ yields the nitrosyl carbonyl cluster $[FeRu_3(CO)_{12}(NO)]^-$. The rate of this reaction shows a first-order dependence on the concentration of $Ru_3(CO)_{12}$ and is inhibited by addition of excess CO. A single-crystal X-ray crystallographic analysis of $PPN[FeRu_3(CO)_{12}(NO)]$ [$P2_1/c$ space group, a = 19.690 (4) Å, b = 16.262 (3) Å, c = 15.911 (5) Å, β = 107.24 (2)°, Z = 4] revealed that the $FeRu_3$ tetrahedral core contained a terminal, linear nitrosyl ligand bound to the iron. Three carbonyls bridge the three iron–ruthenium bonds such that the overall symmetry is C_3. $[FeRu_3(CO)_{12}(NO)]^-$ cleanly reacts to form CO_2 and the nitrido cluster $[FeRu_3N(CO)_{12}]^-$. A structural analysis of the Et_4N^+ salt of this cluster [$P\bar{1}$] space group, a = 12.464 (1) Å, b = 12.697 (1) Å, c = 9.437 (2) Å, α = 94.40 (2)°, β = 100.17 (2)°, γ = 107.75 (1)°, Z = 2] revealed that it has a butterfly framework of metal atoms with the nitrogen coordinated to all four metals. Three terminal carbonyl ligands are also coordinated to each metal. The iron is disordered over all four sites in the structure which means that two isomeric forms exist and cocrystallize. Isomer I contains Fe in the wing-tip position while the other (II) contains Fe in the hinge position. Solution spectroscopic evidence (infrared, ^{13}C NMR and ^{15}N NMR) shows that both isomers persist in solution. Measurement of the equilibrium constant for the isomerization, I ⇄ II, at several temperatures between 25 and 68 °C yielded $\Delta H = -3.5 + 1.0$ kcal/mol and $\Delta S = -13 \pm 2$ eu. The rate of conversion of I → II at 25 °C is $(4.2 \pm 0.2) \times 10^{-7}$ s^{-1}. Possible mechanisms for this unique isomerization are presented. A kinetic analysis of the deoxygenation of $[FeRu_3(CO)_{12}(NO)]^-$ to give $[FeRu_3N(CO)_{12}]^-$ over the temperature range from 25 to 65 °C revealed that the deoxygenation is first order in cluster concentration. Possible mechanisms of the NO deoxygenation consistent with this and other observations are discussed.

The formation of polynuclear compounds containing main-group interstitial atoms is often a poorly understood process. With some notable exceptions[2,3] the formation of clusters with interstitial atoms also involves changes in the nuclearity of the product. Despite having a reaction that proceeds in high yield, there are often too many bonds being broken and formed to develop a clear understanding of the reaction mechanism. Reaction 1, which is an excellent synthetic reaction, exemplifies the problems faced in such a study.[4] The CO bond cleavage step (the point of exceptional interest) is just one of many involved in product formation.

$$Fe(CO)_5 + Fe(CO)_4^{2-} \rightarrow [Fe_6C(CO)_{16}]^{2-} \quad (1)$$

Like the source of carbon in many carbido clusters[5] the source of nitrogen in nitrido clusters is derived from its monoxide.[6-13]

(1) Fellow of the Alfred P. Sloan Foundation (1983–1985).
(2) Hayward, C. M. T.; Shapley, J. R. *Inorg. Chem.* **1982**, *21*, 3816.
(3) Kolis, J. W.; Holt, E. M.; Drezdon, M.; Whitmire, K. H.; Shriver, D. F. *J. Am. Chem. Soc.* **1982**, *104*, 6134.
(4) Tachikawa, M.; Geerts, R. L.; Muetterties, E. L. *J. Organomet. Chem.* **1981**, *213*, 11.
(5) Tachikawa, M.; Muetterties, E. L. *Prog. Inorg. Chem.* **1981**, *28*, 203.
(6) Martinengo, S.; Ciani, G.; Sironi, A.; Heaton, B. T.; Mason, J. *J. Am. Chem. Soc.* **1979**, *101*, 7095.

0002-7863/84/1506-4799$01.50/0

Table I. Spectroscopic Data

compound	color	infrared (1600–2200 cm^{-1}), cm^{-1}	^{13}C,[a] ppm (rel to Me_4Si)	^{15}N, ppm (rel to NH_3)
$[FeRu_3(CO)_{12}(NO)]^-$	red	2066 m, 2022 vs, 1978 s, 1823 m, 1786 m, 1736 w (ν_{NO}) for ^{15}N: 1705 w (THF)	212.2 (−90 to +25 °C THF)	391.4 (CH_2Cl_2)
$[FeRu_3N(CO)_{12}]^-$ (Fe = wing-tip, I)	red	2064 w, 2023 s, 2000 vs, 1964 m, 1950 sh (THF)	+27 °C: 214.0 (3), 200.2 (6), 198.1 (3) −100 °C: 213.7 (3), 205.3 (2), 204.8 (2), 203.7 (1), 194.6 (2), 189.8 (2) (THF)	559.2 (CH_2Cl_2)
mixture of I and II obtained in synthesis		2063 w, 2036 s, 2023 s, 2001 vs, 1986 s, 1981 sh, 1975 sh, 1936 sh, 1909 w (THF)		
$[FeRu_3N(CO)_{12}]^-$[b] (Fe = hinge, II)	red	2063 w, 2036 s, 2001 s, 1985 s, 1970 sh, 1937 vw, 1909 w (THF)	+27 °C: 216.2 (3), 201.7 (3), 197.6 (6) −100 °C: 215.9 (3), 205.8 (2), 203.3 (2), 195.2 (2), 193.3 (2), 192.9 (1) (THF)	520.1 (CH_2Cl_2)
$[FeRu_4N(CO)_{12}]^-$	red	2061 w, 2012 vs, 2003 sh, 1986 s, 1960 sh, 1914 vw, 1820 w (THF)	213.0 (3), 204.6 (11) (−90 to +25 °C, THF)	

[a] Chemical shifts are subject to a small temperature dependence. [b] Pure isomer II was prepared by reacting a mixture of both isomers with $P(OCH_3)_3$. Only I reacts and the substituted cluster can be separated leaving pure II. Details of this will be published separately.

The first examples of low-valent nitrido clusters were prepared by using the nitrosonium ion (eq 2 and 3).[6] The iron nitrido

$$Co_6(CO)_{15}^{2-} + NO^+ \rightarrow Co_6N(CO)_{15}^- \quad (2)$$

$$Rh_6(CO)_{15}^{2-} + NO^+ \rightarrow Rh_6N(CO)_{15}^- \quad (3)$$

clusters $[Fe_4N(CO)_{12}]^-$ and $[Fe_5N(CO)_{14}]^-$ were also synthesized[7] by using NO^+, and recently this method has been applied to $HRu_4N(CO)_{12}$,[8] $H_3Ru_4N(CO)_{11}$,[9] $HOs_4N(CO)_{12}$,[9] and $CoRu_3N(CO)_{12}$.[10] These reactions are likely to proceed through clusters containing a coordinated nitric oxide ligand. This has been shown in the conversion of $H_3Os_4(CO)_{12}(NO)$ to $HOs_4N(CO)_{12}$[9] and also in a preliminary communication of this work.[11]

The synthesis of nitrido clusters by the condensation of monomeric nitrosyl complexes was first reported for reaction 4.[11,12]

$$3Fe_3(CO)_{12} + 2[Fe(CO)_3(NO)]^- \rightarrow 2[Fe_4N(CO)_{12}]^- + CO + 2CO_2 + 3Fe(CO)_5 \quad (4)$$

Recently the trinuclear Mo and W clusters $(\eta^5\text{-}C_5H_5)_3M_3(O)(\eta_3\text{-}N)(CO)_4$ as well as the mixed-metal systems were isolated from the pyrolysis of $(\eta^5\text{-}C_5H_5)M(CO)_2(NO)$ with the dinuclear species $(\eta^5\text{-}C_5H_5)_2M_2(CO)_6$ at 170 °C.[13]

The only example of a nitrido cluster that does not have NO as the ultimate source of the nitrogen is $[Ru_6N(CO)_{16}]^-$.[14] This was prepared in nearly quantitative yield from reaction 5, which involves intermediate clusters containing an isocyanato ligand.

$$2Ru_3(CO)_{12} + N_3^- \rightarrow [Ru_6N(CO)_{16}]^- + 8CO + N_2 \quad (5)$$

With the exception of the last reaction, it is the cleavage of the N–O bond of a coordinated nitrosyl that generates nitrido clusters. This same N–O bond cleavage is also important in the heterogeneous catalyzed reactions of NO (eq 6 and 7).[15]

$$2NO + CO \rightarrow N_2O + CO_2 \quad (6)$$

$$2NO + 5H_2 \rightarrow 2NH_3 + 2H_2O \quad (7)$$

What is known about the cleavage of the NO bond (or for that matter cleavage of the CO bond involved in carbido cluster preparation)? Due to the problems mentioned, essentially nothing is known. We present in this paper the first complete study characterizing the deoxygenation of a cluster coordinated NO ligand. The solid-state and solution structure of both the starting material and the product are included as well as a kinetic analysis of this reaction.

Experimental Section

PPN$[Fe(CO)_3(NO)]$[16] (PPN = bis(triphenylphosphine)nitrogen(1+) cation) and $Ru_3(CO)_{12}$[17] were prepared according to published procedures. Tetrahydrofuran (THF) and diethyl ether were distilled from sodium benzophenone ketyl, CH_2Cl_2 was distilled from P_2O_5, and hexane was distilled from sodium metal prior to use. Other reagents purchased from commercial sources were used as received. All reactions were carried out under an N_2 atmosphere. Infrared spectra were recorded on a Beckman Model No 4250 spectrophotometer, and the nmr data were recorded on a Nicolet NTCFT-1180 300-MHz spectrophotometer. The samples for the ^{15}N NMR experiments were prepared from $Na^{15}NO_2$ (95% enriched) obtained from Merck, Sharp and Dohme. Each ^{15}N NMR spectrum was conducted with CH_2Cl_2 as the solvent (3.0 mL) in a 12-mm tube with sample concentrations between 0.03 and 0.05 M and $Cr(acac)_3$ (53 mg) added. The referencing was done externally by using CH_3NO_2 in CH_2Cl_2 with 0.03 M $Cr(acac)_3$ set at 379.60 ppm downfield from NH_3 (liquid, 25 °C).[18] All data are reported relative to NH_3. With an acquisition time of 0.68 s, a good signal-to-noise ratio was obtained with ~2000 scans. A summary of the spectroscopic data of the compounds is given in Table I.

Preparation of PPN$[FeRu_3(CO)_{12}(NO)]$. PPN$[Fe(CO)_3(NO)]$ (70.6 mg, 0.0996 mmol) and $Ru_3(CO)_{12}$ (184 mg, 0.288 mmol) were placed in a round-bottom flask equipped with a condenser. THF (50 mL) was added by syringe, and the solution was brought to reflux. The reflux was maintained for 15 min, and then the THF was pumped off immediately while still hot. After the THF was removed, 25 mL of diethyl ether was added to the solid residue and the solution was filtered. Addition of 25 mL of hexane to the filtrate (with rapid stirring) caused crystals to form. The crystals were redissolved in 30 mL of diethyl ether, layered with 30 mL of hexane, and left in a freezer (−25 °C) to crystallize. After 3 days the crystals that had formed were filtered and washed with cold diethyl ether to give 51 mg (0.04 mmol, 41% yield) of red, crystalline PPN$[FeRu_3(CO)_{12}(NO)]$. Anal. Calcd for PPN$[FeRu_3(CO)_{12}(NO)]$: C, 45.62, H, 2.22; N, 2.39. Found: C, 45.87; H, 2.46; N, 2.41.

Preparation of PPN$[FeRu_3N(CO)_{12}]$. PPN$[Fe(CO)_3(NO)]$ (199.5 mg, 0.282 mmol) and $Ru_3(CO)_{12}$ (192 mg, 0.300 mmol) were put in a Schlenk tube, and 30 mL of THF was added by syringe. This solution was brought to reflux that was maintained for 80 min. The THF was then removed under vacuum, 40 mL of ether was added, and the reaction vessel was put under a CO atmosphere for 2 h. After the Schlenk tube was purged with N_2, the solution was filtered and the product was crystallized by adding an equal volume of hexane to the rapidly stirred Et_2O solution. This gave 258 mg of red-orange crystals of PPN$[FeRu_3N(CO)_{12}]$ (0.207 mmol, 73% yield).

Preparation of $Et_4N[Fe(CO)_3(NO)]$. $Et_4N(Br)$ (1.0 g, 4.76 mmol) and $NaNO_2$ (303 mg, 4.39 mmol) were dissolved in 10 mL of distilled water and degassed. To this was added 15 mL of THF followed by 2 mL (14.9 mmol) of $Fe(CO)_5$. The two-phase reaction was stirred vigorously for 20 h. The stirring was stopped and the solution allowed to separate.

(7) Tachikawa, M.; Stein, J.; Muetterties, E. L.; Teller, R. G.; Beno, M. A.; Gebert, E.; Williams, J. M. *J. Am. Chem. Soc.* **1980**, *102*, 6648.
(8) Braga, D.; Johnson, B. F. G.; Lewis, J.; Mace, J. M.; McPartlin, M.; Puga, J.; Nelson, W. J. H.; Raithby, P.; Whitmire, K. H. *J. Chem. Soc., Chem. Commun.* **1982**, 1081.
(9) Collins, M. A.; Johnson, B. F. G.; Lewis, J.; Mace, J. M. Morris, J.; McPartlin, M.; Nelson, W. J. H.; Puga, J.; Raithby, P. R. *J. Chem. Soc., Chem. Commun.* **1983**, 689.
(10) Fjare, D. E.; Keyes, D. G.; Gladfelter, W. L. *J. Organomet. Chem.* **1983**, *250*, 383.
(11) Fjare, D. E.; Gladfelter, W. L. *J. Am. Chem. Soc.* **1981**, *103*, 1572.
(12) Fjare, D. E.; Gladfelter, W. L. *Inorg. Chem.* **1981**, *20*, 3533.
(13) Feasey, N. D.; Knox, S. A. R. *J. Chem. Soc., Chem. Commun.* **1982**, 1062.
(14) Blohm, M. L.; Fjare, D. E.; Gladfelter, W. L. *Inorg. Chem.* **1983**, *22*, 1004.
(15) Eisenberg, R.; Hendricksen, D. E. *Adv. Catal.* **1979**, *28*, 79.
(16) Stevens, R. E.; Gladfelter, W. L. *Inorg. Chem.* **1983**, *22*, 2034.
(17) Mantovani, A.; Cenini, S. *Inorg. Synth.* **1976**, *16*, 47.
(18) Levy, G. C.; Lichter, R. L. "Nitrogen-15 Nuclear Magnetic Resonance Spectroscopy"; Wiley: New York, 1979.

With use of cannula, the yellow organic layer was decanted and filtered through $MgSO_4$, and then the THF was removed under vacuum. The solid residue was washed with diethyl ether until the filtrate was pale yellow and bright yellow crystals of $Et_4N[Fe(CO)_3(NO)]$ (841 mg, 64% yield) remained.

Preparation of $Et_4N[FeRu_3N(CO)_{12}]$. $Et_4N[Fe(CO)_3(NO)]$ (120.4 mg, 0.401 mmol) and $Ru_3(CO)_{12}$ (270.7 mg, 0.424 mmol) were reacted by using the same procedure described for the PPN^+ salt. $Et_4N[FeRu_3N(CO)_{12}]$ (235 mg, 70% yield) was recrystallized from CH_2Cl_2/hexane. Anal. Calcd for $Et_4N[FeRu_3N(CO)_{12}]$: C, 28.62; H, 2.40; N, 3.34. Found: C, 28.55; H, 2.34; N, 3.30.

Preparation of $PPN[FeRu_4N(CO)_{14}]$. $PPN[FeRu_3N(CO)_{12}]$ (560 mg, 0.45 mmol) and $Ru_3(CO)_{12}$ (100 mg, 156 mmol) were dissolved in 60 mL of THF and heated at reflux for 50 h until the infrared absorbances due to $[FeRu_3N(CO)_{12}]^-$ were no longer visible. The THF was removed under vacuum, 50 mL of ether was added, and the solution was filtered. Hexane (50 mL) was gently layered over the ether. After 2 days an oil had formed, but in ~1 week crystals were visible. These crystals were removed and washed with hexane to give 65 mg of red plate-shaped crystals of $PPN[FeRu_4N(CO)_{14}]$ (0.046 mmol, 10%). The remaining oil can be recrystallized in the same manner to give additional crystals of $PPN[FeRu_4N(CO)_{14}]$: mass spectrum (FAB, negative ion), m/e 870 (parent ion, ^{102}Ru). Anal. Calcd for $PPN[FeRu_4N(CO)_{14}]$: C, 42.75; H, 2.15; N, 1.99. Found: C, 43.39; H, 2.48; N, 1.77.

$PPN[FeRu_3(CO)_{12}(NO)]$ + CO. $PPN[FeRu_3(CO)_{12}(NO)]$ (8.5 mg, 6.7 μmol) was dissolved in 4 mL of THF and put under a CO atmosphere at 25 °C. During the reaction only $[FeRu_3(CO)_{12}(NO)]^-$, $[Fe(CO)_3(NO)]^-$, and $Ru_3(CO)_{12}$ were observable by IR spectroscopy. The conversion of $[FeRu_3(CO)_{12}(NO)]^-$ into $[Fe(CO)_3(NO)]^-$ and $Ru_3(CO)_{12}$ had a half-life of about 45 min under these conditions.

$PPN[FeRu_3(CO)_{12}(NO)]$ + $P(OCH_3)_3$. $PPN[FeRu_3(CO)_{12}(NO)]$ (10.5 mg, 8.3 μmol) was dissolved in 5 mL of THF, and 22 μL of $P(OCH_3)_3$ (0.17 mmol) was added by syringe. The infrared spectrum after $^1/_2$ h showed that $[FeRu_3(CO)_{12}(NO)]^-$ had been consumed. In the terminal CO region a strong peak at 1980 cm^{-1} with a shoulder at 2000 cm^{-1} and a medium intensity peak at 2020 cm^{-1} were present. Peaks at 1878 and 1650 cm^{-1} due to $[Fe(CO)_3(NO)]^-$ and much smaller peaks at 1833 and 1618 cm^{-1} possibly from $[Fe(CO)_2(P(OCH_3)_3)(NO)]^-$ had also appeared. Over 20 h, the peaks at 2020, 1833, and 1618 cm^{-1} slowly disappeared and the peaks at 2000 (sh), 1980, 1878, and 1650 cm^{-1} slowly continued to grow. The infrared spectrum after 20 h showed only $[Fe(CO)_3(NO)]^-$ and $Ru_3(CO)_9(P(OCH_3)_3)_3$, the latter product being identified (after extraction into hexane) by its infrared and ^1H NMR spectra.[19]

Kinetic Analysis of the Reaction of $PPN[Fe(CO)_3(NO)]$ with $Ru_3(CO)_{12}$ in Tetrahydrofuran. In a typical experiment, $PPN[Fe(CO)_3(NO)]$ and $Ru_3(CO)_{12}$ were accurately weighed and put in the reaction vessel. The initial concentration of $[Fe(CO)_3(NO)]^-$ was then determined from a calibration curve of percent transmittance (ν_{NO} at 1651 cm^{-1}) vs. concentration, and the initial concentration of $Ru_3(CO)_{12}$ was calculated from the molar ratio of the two reagents. The solution was then immersed in a hot oil bath, bringing it to reflux. The reaction was monitored by measuring the disappearance of the ν_{NO} peak at 1651 cm^{-1} in the infrared spectrum. The concentration of $Ru_3(CO)_{12}$ during the reaction was calculated by assuming it reacts with $[Fe(CO)_3(NO)]^-$ in a 1:1 ratio, the experimentally determined stoichiometry. Triplicate runs of three different concentrations of the reactants, followed for at least 2 half-lives, gave good agreement with an average $k = (6.5 \pm 0.2) \times 10^{-4}$ s^{-1}. In a tenth experiment run under a CO atmosphere the observed rate was inhibited, $k = 2.5 \times 10^{-4}$ s^{-1}. A typical plot of ln $[Ru_3(CO)_{12}]$ vs. time is shown in Figure 1. The concentration of $[Fe(CO)_3(NO)]^-$ was varied from 2.36 to 5.17 mM in these experiments.

Kinetic Analysis of the Conversion of $PPN[FeRu_3(CO)_{12}(NO)]$ to $PPN[FeRu_3N(CO)_{12}]$. In a typical experiment a solution of $[FeRu_3(CO)_{12}(NO)]^-$ in tetrahydrofuran was prepared and its concentration was determined from a calibration curve of percent transmittance vs. concentration (based on the bridging ν_{CO} at 1823 cm^{-1}). The solution was placed in a specially designed Schlenk tube equipped with a built-in condenser (to minimize evaporation problems), and the Schlenk tube was immersed in a thermostated water bath where the temperature was automatically maintained to ±0.2 °C. Samples were withdrawn, and the reaction was monitored by measuring the disappearance of the 1823 cm^{-1} peak in the infrared spectrum. Triplicate runs were performed at five different temperatures from 25 to 65 °C and also in refluxing THF (~68 °C). The reactions were followed for at least 2 half-lives and were in excellent agrement at each temperature. The reaction followed simple first-order kinetics, and the average rate values are listed in the supplementary material. A typical plot of ln $[FeRu_3(CO)_{12}(NO)]$ vs. time is shown in Figure 2. The activation parameters calculated from these values of k are $\Delta H^* = 26.4 \pm 0.4$ kcal/mol and $\Delta S^* = +3.9 \pm 1.3$ eu.

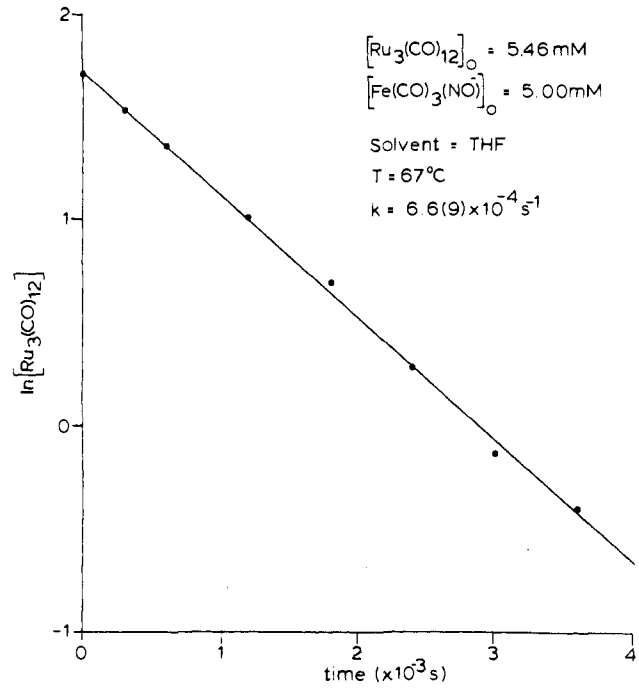

Figure 1. Plot of ln $[Ru_3(CO)_{12}]$ vs. time for the reaction of $Ru_3(CO)_{12}$ with $PPN[Fe(CO)_3(NO)]$.

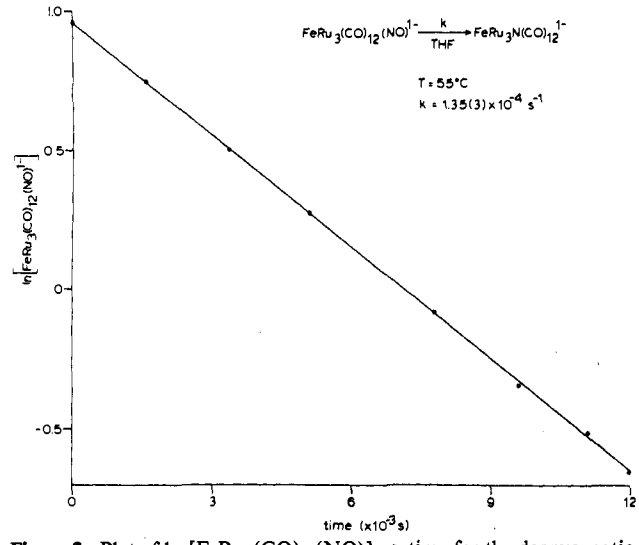

Figure 2. Plot of ln $[FeRu_3(CO)_{12}(NO)]$ vs. time for the deoxygenation of $PPN[FeRu_3(CO)_{12}(NO)]$.

Thermodynamic Analysis of the Interconversion of the Two Isomers of $PPN[FeRu_3N(CO)_{12}]$. Six identical NMR tubes of $PPN[FeRu_3N(CO)_{12}]$, enriched with ^{13}CO, were prepared by dissolving 193 mg of $PPN[FeRu_3N(*CO)_{12}]$ and 52.5 mg of $Cr(acac)_3$ in 3 mL of THF. A 0.5-mL sample of this solution was transferred into six 5-mm NMR tubes that were then sealed under a N_2 atmosphere. These tubes were kept in constant temperature baths at six temperatures from 25 to 68 °C until they had reached equilibrium. The ^{13}C NMR spectra were recorded, and the ratio $K_{eq} = II/I$ was determined by integrating the carbonyl resonances. With an acquisition time of 0.82 s, a good signal-to-noise ratio was obtained with ~1000 scans. These results are summarized in Table II, and a plot of ΔG vs. T is shown in Figure 3. From these data $\Delta H = -3.5 \pm 1.0$ kcal/mol and $\Delta S = -13 \pm 2$ eu.

Kinetic Analysis of the Interconversion of the Two Isomers of $PPN[FeRu_3N(CO)_{12}]$. A sample of isomer I enriched with ^{13}CO was prepared by deprotonating $HFeRu_3N(*CO)_{12}$ and methathesizing with PPN[Cl]. The cluster was dissolved in THF, with $Cr(acac)_3$ (0.03 M) added as a shiftless relaxation reagent, and sealed in a 5-mm NMR tube under N_2. The NMR tube was kept in a thermostated water bath at 27 ± 0.2 °C and periodically withdrawn to sample the ^{13}C NMR spectrum. With an

(19) Bruce, M. I.; Shaw, G.; Stone, F. G. A. *J. Chem. Soc., Dalton Trans.* **1972**, 2094.

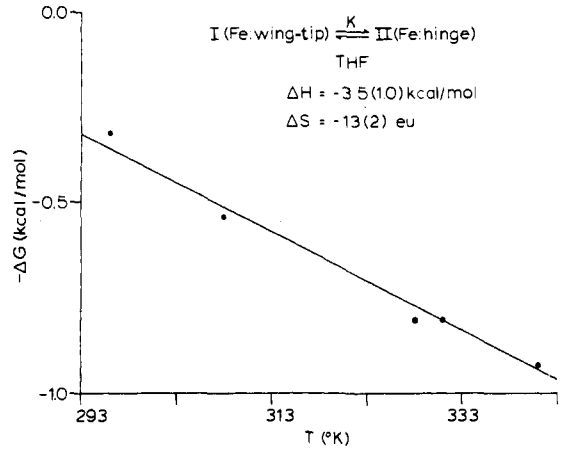

Figure 3. Plot of equilibrium data for the isomerization of $[FeRu_3N(CO)_{12}]^-$.

Table II. Equilibrium Constants for the Isomerization of I ⇄ II in THF

temp, °C	K_{eq} = [II]/[I]	ΔG, kcal/mol
23	0.578	0.32
35	0.415	0.54
55	0.290	0.81
58	0.292	0.81
68	0.271	0.91

acquisition time of 0.75 s, a good signal-to-noise ratio was obtained with ~5000 scans. The ratio between the two isomers was determined by integrating the carbonyl resonances. The data were treated as a first-order equilibrium process[20] and are included as supplementary material. From the thermodynamic analysis of the equilibrium, χ_{II} (eq) is known to be equal to 0.340 at 27 °C. A plot (Figure 4) of $+\ln(0.340 - \chi_{II}(t))$ vs. time gives a line with slope $-k_f/0.34$ and an intercept of $-\ln(0.34 - \chi_{II}(0))$. The plot yielded a value for k_f at 27 °C of $(4.2 \pm 0.2) \times 10^{-7}$ s^{-1}. In a second experiment the isomerization of a sample that was initially at equilibrium at 25 °C and then heated to 65 °C was monitored by infrared spectroscopy. Alongside this experiment was an identical solution that was placed under a CO atmosphere at 65 °C. No inhibition of the rate of isomerization could be detected.

Variable-Temperature ^{13}C NMR Study of PPN[$FeRu_3(^*CO)_{12}(NO)$]. PPN[$FeRu_3(CO)_{12}(NO)$] was prepared as previously described except that $Ru_3(CO)_{12}$ enriched in ^{13}CO was used. The enriched $Ru_3(CO)_{12}$ was prepared by stirring 402 mg (0.63 mmol) of $Ru_3(CO)_{12}$ under 250 mL of ^{13}CO (11 mmol) for 2 days at 80 °C. The NMR sample was prepared by placing $Cr(acac)_3$ (50 mg) and PPN[$FeRu_3(CO)_{12}(NO)$] (54 mg) in a 12-mm NMR tube, then distilling in 3 mL at THF, and sealing the tube under vacuum. With use of an acquistion time of 0.31 s and 400 acquisitions, excellent signal-to-noise ratio was achieved at 25 °C. One peak at 212.2 ppm was observed (referenced against proteo-THF, 68.0, 26.3 ppm). At −90 °C the single peak was broadened, $\nu_{1/2}$ ~450 Hz, but was still fairly symmetric. No bridging CO resonances were visible at −90 °C. At −100 °C, the major peak at 209.3 ppm was beginning to sharpen and a very broad shoulder on the low field side of this peak had appeared. This was the lowest temperature attempted.

Pyrolysis of PPN[$FeRu_3(CO)_{12}(NO)$]. Initial Product Study. The NMR tube described in the variable-temperature study of PPN[$FeRu_3(CO)_{12}(NO)$] was heated for 30 min at 67 °C and then cooled to 25 °C and the ^{13}C NMR spectrum recorded. Integration of the carbonyl peak due to $[FeRu_3(CO)_{12}(NO)]^-$ vs. the carbonyl peaks due to $[FeRu_3N(CO)_{12}]^-$ gave a ratio of 0.75:1, indicating the reaction had gone through 1.33 half-lives as predicted by the rate data for this conversion. Integration of the carbonyl peaks due to $[FeRu_3N(CO)_{12}]^-$ (isomer I) vs. those due to isomer II gave a ratio of 2.1:1. Correcting for the conversion of I to II that occurs during the pyrolysis, the ratio of initial product formation (I/II) is 2.0:1.

Variable-Temperature ^{13}C NMR of PPN[$FeRu_3N(CO)_{12}$]. In this experiment, one of the NMR tubes (from the 35 °C point) from the thermodynamic analysis of the interconversion of the two isomers of $[FeRu_3N(CO)_{12}]^-$ was used. The temperature was varied from −100 to +25 °C. With an acquisition time of 0.75 s, good signal-to-noise ratio was obtained in ~500 scans.

(20) Wilkins, R. G. "The Study of Kinetics and Mechanism of Transtion Metal Complexes"; Allyn and Bacon: Boston, 1974; pp 16–17.

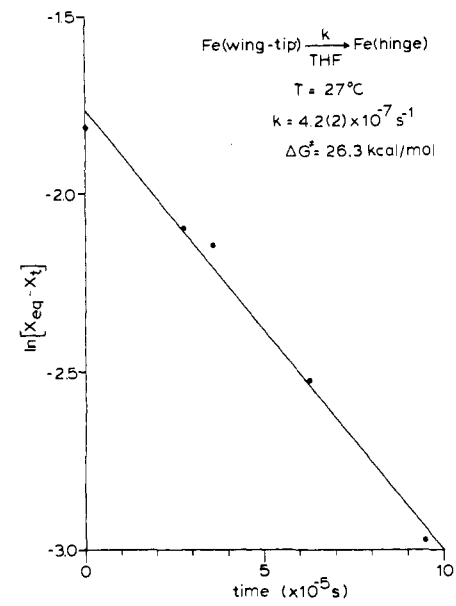

Figure 4. Plot used to derive the rate of isomerization. $\chi_{II,e}$ is the mole fraction of isomer II (Fe = hinge) at equilibrium, and $\chi_{II,t}$ is the mole fraction of II at time t.

Collection and Reduction of the X-ray Data. PPN[$FeRu_3(CO)_{12}(NO)$]. Red crystals were grown from a solution of diethyl ether and hexane. A suitable crystal with dimensions 0.16 × 0.16 × 0.31 mm was mounted on a glass fiber, and preliminary cell data were determined by using rotation and Wiessenberg photographs. The space group $P2_1/c$ was determined unambiguously from the systematic absences at ($0k0$, $k = 2n + l$; $h0l$, $l = 2n + 1$). The crystal was placed on the diffractometer and centered, oriented, and indexed by using the Enraf-Nonius CAD4-SDP programs.[21] The data collection was begun, and a summary of the crystal and intensity measurement parameters is presented in Table III. Background counts were measured at both ends of the scan range with the use of an ω-2θ scan, equal at each side to one-fourth of the scan range of the peak. In this manner, the total duration of measuring background is equal to half of the time required for the peak scan. The check reflections showed no significant decay throughout the entire data collection. The data were corrected for Lorentz, polarization, and background effects.[22] The numerical absorption correction used is based on the Gaussian integration formula.[21] The range of transmission was from 0.805 to 0.842, and the defining faces were ± [(110, 0.078 mm), ($\bar{1}$10, 0.078 mm), and (001, 0.156 mm)].

Et_4N[$FeRu_3N(CO)_{12}$]. Dark red crystals were grown from a solution of CH_2Cl_2/hexane. A suitable, approximately equidimensional (0.2-mm) crystal was chosen and mounted on a glass fiber. The crystal was found to be triclinic by the Enraf-Nonius CAD4-SDP peak search, centering, and indexing programs and by a Delauney reduction calculation.[21] The centric space group $P\bar{1}$ was chosen, and data collection was begun. Table III summarizes the crystal data and intensity measurement parameters. The background was measured in the same fashion described for PPN-[$FeRu_3(CO)_{12}(NO)$]. The check reflections indicated no decay throughout the entire data collection.[22] The data were corrected for Lorentz, polarization, and background effects but not for absorption. The difference between the maximum and minimum transmission was 4.8%.

Solution and Refinement of the Structures. PPN[$FeRu_3(CO)_{12}(NO)$]. The structure was solved by conventional heavy-atom techniques. The positions of the three ruthenium atoms were located by a Patterson

(21) All calculations were carried out on PDP 8A and 11/34 computers using the Enraf-Nonius CAD 4-SDP programs. This crystallographic computing package is described in: Frenz, B. A. In "Computing in Crystallography"; Schenk, H., Olthof-Hazekamp, R., van Koningsveld, H., Bassi, G. C., Eds.; Delft University Press: Delft, Holland, 1978; pp 64–71. See also: "CAD 4 and SDP User's Manual"; Enraf-Nonius: Delft, Holland, 1978.

(22) The intensity data were processed as described: "CAD 4 and SDP User's Manufal"; Enraf-Nonius: Delft, Holland, 1978. The net intensity $I = (K/NPI)(C - 2B)$, where K = 20.1166 × (attenuator factor), NPI = ratio of fastest possible scan rate to scan rate for the measurement, C = total count, and B = total background count. The standard deviation in the net intensity is given by $\sigma^2(I) = (K/NPI)^2[C + 4B + (pI)^2]$, where p is a factor used to downweight intense reflections. The observed structure factor amplitude F_o is given by $F_3 = (I/Lp)^{1/2}$, where Lp = Lorentz and polarization factors. The $\sigma(I)$'s were converted to the estimated errors in the relative structure factors $\sigma(R_o)$ by $\sigma(R_o) = {}^1/_2(\sigma(I)/I)F_o$.

Table III. Summary of Crystallographic Data

	PPN[$FeRu_3$-$(CO)_{12}(NO)$]	Et_4N-[$FeRu_3N(CO)_{12}$]
	Crystal Parameters	
cryst system	monoclinic	triclinic
space group	$P2_1/c$	$P\bar{1}$
a, Å	19.690 (4)	12.464 (1)
b, Å	16.262 (3)	12.697 (1)
c, Å	15.911 (5)	9.437 (2)
α, deg	90	94.40 (2)
β, deg	107.24 (2)	100.17 (2)
γ, deg	90	107.75 (1)
V, Å^3	4866 (4)	1386.4 (9)
Z	4	2
d(calcd), g cm^{-3}	1.73	2.01
temp, °C	23	23
abs coeff, cm^{-1}	13.5	21.5
	Measurement of Intensity Data	
diffractometer	Enraf-Nonius CAD4	Enraf-Nonius CAD4
radiation	Mo Kα (λ = 0.71073 Å)	Mo Kα (λ = 0.71073 Å)
monochromator	graphite crystal	graphite crystal
scan type	ω–2θ	ω–2θ
scan speed (variable from), deg/min	0.38–20.0	2.35–20
scan range, deg	$0 \le 2\theta \le 56$	$0 \le 2\theta \le 54$
reflcns measd	$\pm h,+k,+l$	$\pm h,\pm k,+l$
check reflcns	{1000}, {0100}, {008}; measd approximately every 120 reflcns	{800}, {080}, {22$\bar{7}$}; measd approximately every 150 reflcns
reflcns collected	11698 unique reflcns; 7125 with $I > 2\sigma(I)$	5442 unique reflcns; 4358 with $I > 2.5\sigma(I)$
p	0.06	0.03
R	0.046	0.022
R_w	0.068	0.028
error in observn of unit	1.718	1.171

synthesis. Following three cycles of least-squares refinement of the ruthenium atom positions and isotropic thermal parameters, a difference Fourier calculation revealed the position of the Fe, the P–N–P linkage of the cation, and several CO ligands. Subsequent refinement and difference Fourier maps resulted in the location of all non-hydrogen atoms.[23] At this point the terminal ligand on the iron was assigned as the nitrosyl ligand due to the shortened (1.67 Å) Fe–X bond. All atoms of the anion and the PNP atoms of the cation were refined by using anisotropic thermal parameters. The carbon atoms of the cation were refined isotropically, and the hydrogen atoms were not included. After convergence the assignment of the nitrosyl location was checked by replacing the N with a C, refining the structure, and examining the thermal parameters of this atom compared to the other carbon atoms of the anion. The isotropic equivalent for this atom was originally 4.5 as nitrogen, and it dropped to 3.2 as carbon. This value was significantly lower than each of the other individual carbons of the carbonyl ligands as well as their cumulative average value (4.6 (4)). This test provides strong evidence that the nitrosyl ligand is attached to the iron atom. The final difference Fourier revealed no significant features around the anion and only small peaks (~1.0 e/Å^3) near the carbon atoms of the cation. The values of the atomic scattering factors used in the calculations were taken from the usual tabulation, and the effects of anomalous dispersion were included.[24] Tables IV, V, and VI contain the positional parameters, bond distances, and angles, respectively.

(23) The function minimized was $\sum w(|F_o| - |F_c|)^2$, where $w = 1/\sigma^2(F_o)$. The unweighted and weighted residuals are defined as $R = (\sum||F_o| - |F_c||)/\sum|F_o|$ and $R_w = [(\sum w(|F_o| - |F_c|)^2/(\sum w|F_o|)^2]^{1/2}$. The error in an observation of unit weight is $[\sum w(|F_o| - |F_c|)^2/(NO - NV)]^{1/2}$, where NO and NV are the number of observations and variables, respectively.

(24) Cromer, D. T.; Waber, J. T. "International Tables for X-ray Crystallography"; Kynoch Press: Birmingham, England, 1974; Vol. IV, Table 2.2A. Cromer D. T. *Ibid.*, Table 2.3.1.

(25) Cromer, D. T.; Ibers, J. A. "International Tables for X-ray Crystallography"; Kynoch Press, Birmingham, England, 1984; Vol. IV, Table 2.2C.

$Et_4N[FeRu_3N(CO)_{12}]$. The structure was solved by conventional heavy-atom techniques. The positions of the four metal atoms were located by a Patterson synthesis. Although the unambiguous identification of the iron atom was not possible at this stage, one of the wing-tip metals was labeled as iron. After several cycles of least-squares refinement and difference Fourier calculations, all non-hydrogen atoms were located.[23] The atom labeled as Fe was relabeled as Ru, and the multiplicity of the Ru atom in each site was allowed to refine. During this process all non-hydrogen atoms were refined by using anisotropic temperature factors. Difference Fourier maps eventually revealed the positions of all the H atoms on the cation. These were added to the list but not refined. The multiplicites of the ruthenium atoms were M1, 0.918, M2, 0.899, M2, 0.856, and M4, 0.779. We changed the model to the real formula containing one Fe and three Ru atoms and with use of the multiplicites above calculated the percent iron at each site. Refinement was continued in the following stepwise fashion. Three cycles of least squares were completed by refining only the positional and anisotropic temperature, parameters, the multiplicities of the Ru atoms, the scale factor, and the extinction coefficient. All parameters associated with the Fe were fixed by using the refined Ru parameters. These were changed after each cycle of refinement. The final multiplicites determined from this procedure and corrected for the 1Fe:3Ru formula were as follows: M1, Ru, 0.896, Fe, 0.104; M2, Ru, 0.846, Fe, 0.154; M3, Ru, 0.731, Fe, 0.269, M4, Ru, 0.527, Fe, 0.473. During the final three cycles of refinement the multiplicities were fixed and the parameters of all the atoms were refined to convergence yielding $R = 0.022$ and $R_w = 0.028$.

For evaluation of the significance of the disordered model described above, four additional models were completely refined. The completely ordered model with iron placed at M4 converged to $R = 0.062$ and $R_w = 0.100$ and very small temperature factors for the iron. Refinement based on an equal population of the Fe in the two wing-tip positions improved the fit somewhat ($R = 0.036$, $R_w = 0.054$), while distributing the Fe equally among the two hinge positions worsened the fit ($R = 0.075$, $R_w = 0.115$). Refinement with the Fe equally distributed among all four sites converged to $R = 0.035$ and $R_w = 0.053$. With use of the Hamilton's test for comparing R factors,[26] all of these models are significantly worse than the refinement described above. The values of the atomic scattering factors used in the calculations were taken from the usual tabulation, and the effects of anomalous dispersion were included for the non-hydrogen atoms.[24] The hydrogen atom scattering factors were taken from Cromer and Ibers' list.[25] The positional parameters, bond distances, and bond angles are listed in Tables VII, VIII, and IX, respectively.

Results

Preparation of $[FeRu_3(CO)_{12}(NO)]^-$. The reaction of $[Fe(CO)_3(NO)]^-$ with $Ru_3(CO)_{12}$ proceeds smoothly in refluxing THF (eq 8). Since $[FeRu_3(CO)_{12}(NO)]^-$ will go on to further products,

$$[Fe(CO)_3(NO)]^- + Ru_3(CO)_{12} \rightarrow 3CO + [FeRu_3(CO)_{12}(NO)]^- \quad (8)$$

it is important to carefully control the parameters of the reaction. Excess $Ru_3(CO)_{12}$ enhances the rate of formation of $[FeRu_3(CO)_{12}(NO)]^-$, and although this is the more expensive reagent, it can easily be recovered after the reaction. The time (15 min) is also critical to optimize the yield, as is the temperature which must be maintained at a level that allows a steady reflux rate of the solvent. Even at 60 °C the reaction becomes imperceptably slow since the THF is not refluxing. Pure material can be obtained in overall 41% yield by a slow recrystallization from ether layered with hexane. If any PPN[$FeRu_3N(CO)_{12}$] is formed in the reaction, two different crystals are observed. Both are dark red, but PPN[$FeRu_3(CO)_{12}(NO)$] forms rectangular prismatic crystals while PPN[$FeRu_3N(CO)_{12}$] forms thin plates.

A preliminary kinetic analysis of the reaction of PPN[$Fe(CO)_3(NO)$] with $Ru_3(CO)_{12}$ was conducted in refluxing THF. This information was used primarily to develop the above optimized synthesis of $[FeRu_3(CO)_{12}(NO)]^-$. The reaction was followed for 2 half-lives by observing the intensity of the ν_{NO} of $[Fe(CO)_3(NO)]^-$ peak at 1651 cm^{-1}, and the procedure described in the Experimental Section was developed to minimize contamination from oxygen. Variation of the concentration of $[Fe(CO)_3(NO)]^-$ from 2.36 to 5.17 mM caused no change in the rate of reaction, and excellent correlations were obtained by plotting ln $[Ru_3(CO)_{12}]$ vs. time. Figure 1 shows a typical plot of the data

(26) Hamilton, W. C. *Acta Crystallogr.* **1965**, *18*, 502.

Table IV. Positional Parameters for PPN[$FeRu_3(CO)_{12}(NO)$]

atom	x	y	z	atom	x	y	z
Ru1	0.30982 (2)	0.19230 (3)	−0.00837 (3)	C48	0.4306 (4)	0.6448 (5)	0.4474 (5)
Ru2	0.17999 (2)	0.19772 (3)	0.03623 (3)	C22	0.0456 (4)	0.9755 (5)	−0.2621 (6)
Ru3	0.29281 (2)	0.30460 (3)	0.12092 (3)	C21	0.1138 (4)	0.9735 (5)	−0.2092 (5)
Fe	0.21960 (4)	0.32116 (5)	−0.04982 (5)	C29	0.0920 (4)	0.5469 (5)	−0.3959 (5)
				C35	0.3398 (4)	0.5779 (5)	0.1483 (6)
P1	0.83522 (7)	0.26805 (9)	0.2179 (1)	C45	0.3504 (5)	0.6225 (6)	0.5669 (6)
P2	0.67290 (7)	0.24291 (9)	0.1651 (1)	C26	0.1459 (5)	0.7055 (6)	−0.3940 (6)
				C27	0.1232 (5)	0.6566 (7)	−0.4719 (7)
O	0.1735 (3)	0.4350 (3)	−0.1885 (3)	C36	0.3190 (4)	0.6191 (5)	0.2155 (5)
O2	0.1009 (2)	0.3667 (3)	0.0108 (3)	C47	0.4556 (5)	0.5967 (6)	0.5276 (6)
O1	0.1900 (2)	0.1988 (3)	−0.1875 (3)	C28	0.0982 (4)	0.5812 (6)	−0.4723 (6)
O11	0.2917 (3)	0.1769 (3)	0.2602 (3)	C17	0.1603 (5)	0.5773 (6)	−0.0168 (7)
O4	0.4211 (2)	0.2733 (4)	−0.0781 (3)	C23	0.0108 (5)	0.9089 (6)	−0.3072 (6)
O10	0.2170 (3)	0.4384 (3)	0.1896 (3)	C16	0.0928 (5)	0.5842 (6)	−0.0175 (6)
O3	0.3432 (2)	0.4270 (3)	0.0018 (3)	C15	0.0457 (5)	0.6320 (6)	−0.0708 (6)
O5	0.4184 (3)	0.1308 (4)	0.1595 (3)	C46	0.5854 (5)	0.4105 (6)	0.4202 (6)
O7	0.0869 (3)	0.2003 (4)	0.1583 (4)	C31	0.6469 (3)	0.1925 (3)	0.2512 (4)
O9	0.0609 (3)	0.1321 (4)	−0.1151 (4)	C33	0.5745 (4)	0.1822 (5)	0.3488 (5)
O12	0.4417 (3)	0.3594 (4)	0.2268 (4)	C19	0.8833 (3)	0.1726 (4)	0.2389 (4)
O8	0.2475 (2)	0.0321 (3)	0.1035 (4)	C37	0.6307 (3)	0.3421 (3)	0.1497 (3)
O6	0.3062 (3)	0.0313 (3)	−0.1057 (4)	C43	0.6360 (3)	0.1819 (4)	0.0670 (4)
				C38	0.6690 (3)	0.4083 (4)	0.1952 (4)
N1	0.1924 (3)	0.3884 (3)	−0.1299 (3)	C41	0.5307 (3)	0.4313 (4)	0.0929 (5)
N2	0.7546 (3)	0.2497 (3)	0.1844 (4)	C25	0.8610 (3)	0.3292 (4)	0.3162 (4)
				C32	0.5948 (3)	0.2247 (4)	0.2832 (5)
C11	0.2860 (3)	0.2214 (4)	0.2031 (4)	C34	0.6089 (4)	0.1084 (5)	0.3844 (5)
C7	0.1234 (3)	0.2014 (4)	0.1138 (4)	C14	0.9334 (4)	0.3200 (5)	0.1362 (5)
C2	0.1444 (3)	0.3222 (4)	0.0012 (4)	C44	0.6768 (4)	0.1719 (5)	0.0089 (5)
C1	0.2203 (3)	0.2249 (4)	−0.1192 (4)	C18	0.8148 (4)	0.3750 (5)	0.0791 (5)
C4	0.3802 (3)	0.2433 (4)	−0.0505 (4)	C42	0.4383 (3)	0.8533 (4)	0.4028 (4)
C5	0.3754 (3)	0.1582 (4)	0.1011 (4)	C30	0.1129 (3)	0.5917 (4)	−0.3166 (4)
C3	0.3050 (3)	0.3766 (4)	0.0151 (4)	C20	0.1500 (3)	0.8962 (4)	−0.1978 (4)
C12	0.3863 (3)	0.3392 (5)	0.1850 (4)	C24	0.0465 (4)	0.8300 (5)	−0.2951 (5)
C10	0.2451 (3)	0.3862 (4)	0.1659 (4)	C40	0.4313 (4)	0.9963 (5)	0.3608 (5)
C8	0.2283 (3)	0.0960 (4)	0.0741 (5)	C39	0.3630 (4)	0.9871 (5)	0.3113 (5)
C9	0.1056 (3)	0.1542 (4)	−0.0579 (5)	C13	0.8636 (3)	0.3239 (4)	0.1367 (4)
C6	0.3069 (4)	0.0919 (4)	−0.0698 (4)				

Table V. Bond Distances (Å) for PPN[$FeRu_3(CO)_{12}(NO)$]

Ru1–Ru2	2.850 (1)	N1–O	1.174 (5)
Ru1–Ru3	2.844 (1)	C1–O1	1.153 (6)
Ru1–Fe	2.699 (1)	C2–O2	1.165 (6)
Ru2–Ru3	2.828 (1)	C3–O3	1.174 (5)
Ru2–Fe	2.673 (1)	C4–O4	1.136 (6)
Ru3–Fe	2.685 (1)	C5–O5	1.146 (6)
Fe–N1	1.643 (4)	C6–O6	1.138 (6)
Fe–C1	1.918 (5)	C7–O7	1.148 (6)
Fe–C2	1.888 (5)	C8–O8	1.156 (6)
Fe–C3	1.918 (5)	C9–O9	1.121 (6)
Ru1–C1	2.158 (5)	C10–O10	1.137 (6)
Ru1–C4	1.899 (5)	C11–O11	1.141 (6)
Ru1–C5	1.917 (6)	C12–O12	1.144 (6)
Ru1–C6	1.894 (5)		
Ru2–C2	2.160 (5)		
Ru2–C7	1.894 (5)		
Ru2–C8	1.915 (6)		
Ru2–C9	1.894 (6)		
Ru3–C3	2.122 (5)		
Ru3–C10	1.885 (5)		
Ru3–C11	1.913 (5)		
Ru3–C12	1.907 (6)		

for the reaction. The nine runs, obtained in triplicate for three sets of concentration conditions, yield an average first-order rate constant of 6.6 (9) × 10^{-4} s^{-1}. Under 1.0 atm of CO the rate drops to 2.5 × 10^{-4} s^{-1}.

The reaction of [$FeRu_3(CO)_{12}(NO)$]$^-$ with either CO or $P(OCH_3)_3$ leads quantitatively to separation of iron from the Ru_3 group (eq 9 and 10). At room temperature reaction 9 requires about

$$[FeRu_3(CO)_{12}(NO)]^- + 3CO \rightarrow [Fe(CO)_3(NO)]^- + Ru_3(CO)_{12} \quad (9)$$

$$[FeRu_3(CO)_{12}(NO)]^- + 3P(OCH_3)_3 \rightarrow [Fe(CO)_3(NO)]^- + Ru_3(CO)_9[P(OCH_3)_3]_3 \quad (10)$$

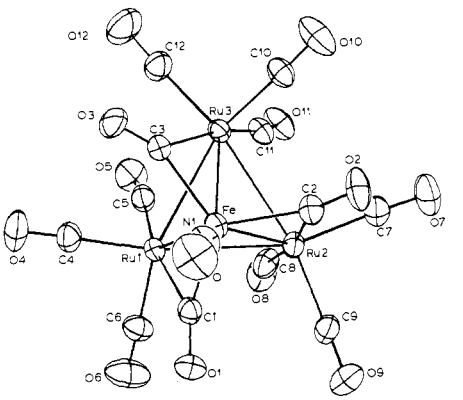

Figure 5. Perspective view of [$FeRu_3(CO)_{12}(NO)$]$^-$ showing the atom labels.

2 h to go to completion. The reaction with phosphite is slower, and infrared data suggest that [$Fe(CO)_2[P(OCH_3)_3](NO)$]$^-$ is formed in the early stages of the reaction. This is evidenced by the appearance of absorbances at 1833 and 1618 cm^{-1} in the infrared spectrum, which show the expected shift relative to the values of 1816 and 1598 cm^{-1} for [$Fe(CO)_2(PPh_3)(NO)$].[27] After the mixture has stirred for 20 h, only [$Fe(CO)_3(NO)$]$^-$ and $Ru_3(CO)_9[P(OCH_3)_3]_3$ are present.

Structure of PPN[$FeRu_3(CO)_{12}(NO)$]. The structure consists of well-separated anions and cations. The $FeRu_3$ core (Figure 5) is tetrahedral with the Ru–Ru and Fe–Ru bond distances averaging 2.84 (1) and 2.69 (1) Å, respectively. The point group of the structure including the ligands closely approximates C_3 with the nitrosyl bonded as a linear ligand (178.1 (4)°) to the iron. Three bridging carbonyls span the three Fe–Ru bonds in a nearly

(27) Roustan, J. L. A.; Forgues, A. *J. Organomet. Chem.* **1980**, *184*, C13.

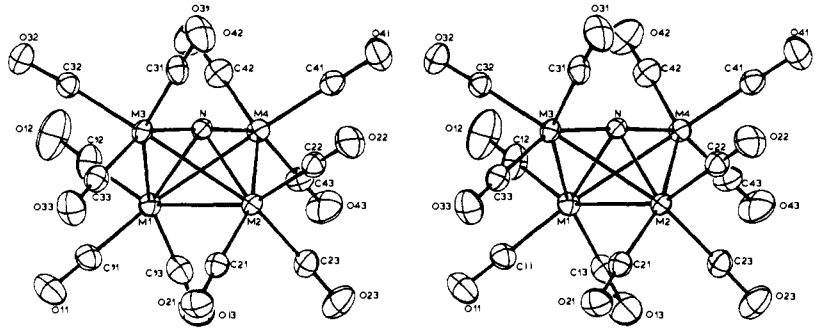

Figure 6. Stereoview of $[FeRu_3N(CO)_{12}]^-$ with the atom labels.

Table VI. Selected Bond Angles (deg) for $PPN[FeRu_3(CO)_{12}(NO)]$

Ru2–Ru1–Ru3	59.56 (1)	C2–Ru2–C8	169.6 (2)
Ru2–Ru1–Fe	57.52 (2)	Ru1–Ru3–Ru2	60.32 (1)
Ru2–Ru1–C1	67.7 (1)	Ru1–Ru3–Fe	58.37 (2)
Ru2–Ru1–C4	151.2 (2)	Ru2–Ru3–Fe	57.94 (3)
Ru2–Ru1–C5	101.3 (2)	Ru2–Ru3–C11	71.8 (2)
Ru2–Ru1–C6	105.2 (2)	Fe–Ru3–C3	45.2 (1)
Ru3–Ru1–Fe	57.87 (2)	C11–Ru3–C3	168.4 (2)
Ru3–Ru1–C1	101.0 (1)	Ru1–Fe–Ru2	64.07 (2)
Ru3–Ru1–C4	103.3 (2)	Ru1–Fe–Ru3	63.76 (2)
Ru3–Ru1–C5	73.8 (2)	Ru1–Fe–N1	138.3 (2)
Ru3–Ru1–C6	159.1 (2)	Ru1–Fe1–C1	52.5 (2)
Fe–Ru1–C1	44.8 (1)	Ru1–Fe–C2	116.4 (2)
Fe–Ru1–C4	94.1 (2)	Ru1–Fe–C3	79.9 (2)
Fe–Ru1–C5	131.6 (2)	Ru2–Fe–Ru3	63.71 (2)
Fe–Ru1–C6	128.7 (2)	Ru2–Fe–N1	145.0 (2)
C1–Ru1–C4	96.3 (2)	Ru2–Fe–C1	74.6 (1)
C1–Ru1–C5	168.7 (2)	Ru2–Fe–C2	53.2 (2)
C1–Ru1–C6	84.1 (2)	Ru2–Fe–C3	114.8 (2)
C4–Ru1–C5	94.7 (2)	Ru3–Fe–N1	143.6 (2)
C4–Ru1–C6	96.2 (3)	Ru3–Fe–C1	114.1 (2)
C5–Ru1–C6	97.4 (2)	Ru3–Fe–C2	79.6 (2)
Ru1–Ru2–Ru3	60.11 (1)	Ru3–Fe–C3	51.7 (2)
Ru1–Ru2–Fe	58.4 (2)	N1–Fe–C1	98.9 (2)
Ru1–Ru2–C8	69.7 (2)	N1–Fe–C2	102.1 (2)
Ru3–Ru2–Fe	58.35 (2)	N1–Fe–C3	97.9 (2)
Fe–Ru2–C2	44.4 (1)	C1–Fe–C2	113.3 (2)
C1–Fe–C3	122.6 (2)	Ru1–C4–O4	178.1 (5)
C2–Fe–C3	116.0 (2)	Ru1–C5–O5	170.4 (5)
Fe–N1–O	178.1 (4)	Ru1–C6–O6	178.8 (5)
Ru1–C1–O1	138.4 (4)	Ru2–C7–O7	176.3 (6)
Fe–C1–O1	138.8 (4)	Ru2–C8–O8	167.5 (5)
Ru2–C2–O2	138.0 (4)	Ru2–C9–O9	176.7 (6)
Fe–C2–O2	139.7 (4)	Ru3–C10–O10	176.2 (4)
Ru3–C3–O3	139.3 (4)	Ru3–C11–O11	169.2 (5)
Fe–C3–O3	137.5 (4)	Ru3–C12–O12	176.9 (5)
Ru1–C8–Ru2	70.9 (2)	P1–N2–P2	168.9 (3)
Ru2–C11–Ru3	69.1 (2)		
Ru3–C5–Ru1	67.7 (2)		

symmetrical fashion. The symmetry of a bridging CO is always difficult to define when different metals are involved. The equivalency of the two M–C–O angles is perhaps the most useful comparison. In $[FeRu_3(CO)_{12}(NO)]^-$ the Fe–C1/2/3–O1/2/3 angles average 139 (1)° that is the same as the average of the Ru1/2/3–C1/2/3–O1/2/3 angles (138.6 (7)°). The NC_3 ligand set of the Fe describes the shape of a trigonal bipyramid with the center of the Ru_3 triangle occupying the remaining axial position. The four carbonyls bonded to each ruthenium atom are located in four octahedral positions, and the fifth position, for instance trans to C6 on Ru1, is taken by another Ru atom (Ru3–Ru1–C6 = 159.1 (2)°). The vectors made by C4/9/10–Ru1/2/3 each intercept a carbon that is coordinated to an adjacent Ru atom, C8/11/5, respectively. These three carbonyls have distances and angles that are significantly different from the other carbonyls and that clearly suggest a weak semibridging interaction. The average Ru–C distances for these three is 1.915 (6) compared to 1.896 (7) Å for the other terminal carbonyls. The long Ru–C distance (Ru1/2/3–C8/11/5) averages 2.89 (6) Å. The Ru–C–O angle is also informative. The three Ru1/2/3–C5/8/11–O5/8/11 angles average 169 (1)° that is significantly less than 177 (1)° for the remaining terminal carbonyls. The last noteworthy point of the structure concerns the PPN cation. The P1–N2–P2 angle is 168.9 (3)°. Although rare examples of linear P–N–P angles exist,[28,29] the vast majority of PPN salts have a value of ~138°.[28,30]

Conversion of $[FeRu_3(CO)_{12}(NO)]^-$. The formation of the nitrido cluster $[FeRu_3N(CO)_{12}]^-$ from the nitrosyl cluster proceeds quantitatively (eq 11). Although CO is required to balance the

$$[FeRu_3(CO)_{12}(NO)]^- + CO \rightarrow [FeRu_3N(CO)_{12}]^- + CO_2 \quad (11)$$

reaction, high yields of the product are formed in the absence of CO. Presumably, this results from a small amount of degradation of the intermediates releasing enough CO to allow good yields to be isolated. The CO_2 released was detected by infrared and ^{13}C NMR spectroscopy. The practical synthesis of $[FeRu_3N(CO)_{12}]^-$ can be conducted starting with either the PPN^+ or Et_4N^+ cations of $[Fe(CO)_3(NO)]^-$ and $Ru_3(CO)_{12}$, and the reaction requires 1.5 h in refluxing THF. For the PPN salt the residue remaining after removal of the THF is extracted into ether leaving $PPN[Fe(CO)_3(NO)]$ and placed under a CO atmosphere to remove any $[FeRu_3(CO)_{12}(NO)]^-$ that may be present. Slow recrystallization from ether/hexane (for PPN^+ salt) or CH_2Cl_2/hexane (for Et_4N^+ salt) generates the product in ~70% yield.

Structure of $Et_4N[FeRu_3N(CO)_{12}]$. The structure of $Et_4N[FeRu_3N(CO)_{12}]$ consists of discrete, ordered Et_4N^+ cations and $[FeRu_3N(CO)_{12}]^-$ anions. Figure 6 shows a stereoview with atom labels for the anion. The overall geometry contains four $M(CO)_3$ groups in a butterfly arrangement where the nitrogen atom is coordinated to each metal so that the local symmetry about the N is C_{2v} (disregarding the differences between the metals). The contacts between the nitrogen and the wing-tip metals are shorter (M3–N 1.872 (2)Å; M4–N 1.846(2) Å) than those to the metals in the hinge positions (M1–N 2.067 (2) Å; M2–N 2.051 (2) Å). The metal–nitrogen–metal angles show that the N is essentially in an octahedral environment with two vacant cis sites. All of the parameters associated with the carbonyls are normal. The dihedral angle between the planes comprised of M1–M2–M3 and M1–M2–M4 is 101.1°. The Et_4N^+ was ordered, and, in fact, all of the hydrogens were located. The N–C distances and the C–C distances averaged 1.523 (5) and 1.504 (5) Å, respectively. While all the N–C–C angles were equivalent (average = 115.9 (4) Å), the C–N–C angles form distinct sets (C50/54–N2–C52/56; average = 106.1 (4) Å; C50/50/52/52–N2–C54/56/54/56, average = 111.2 (3) Å.

The point of overriding interest in this structure regards the disorder of the iron and ruthenium atoms. There are two chemically unique sites in butterfly clusters, the wing-tip positions (M3 and M4) and the hinge positions (M1 and M2). In this space group M3 and M4, as well as M1 and M2, are crystallographically unique. In this structure a partial occupancy for iron can be unambiguously located in each position. This means that both of the possible chemical isomers, I and II, have cocrystallized.

(28) Wilson, R. D.; Bau, R. *J. Am. Chem. Soc.* **1974**, *96*, 7601.
(29) Calderazzo, F.; Englert, U.; Pampaloni, G.; Pelizzi, G.; Zamboni, R. *Inorg. Chem.* **1983**, *22*, 1865.
(30) Pannell, K. H.; Chen, Y.-S.; Belknap, K.; Wu, C. C.; Bernal, I.; Creswick, M. W.; Huang, H. N. *Inorg. Chem.* **1983**, *22*, 418.

Table VII. Positional Parameters for $Et_4N[FeRu_3N(CO)_{12}]$

atom	x	y	z	atom	x	y	z
M1	0.34444 (2)	0.25354 (2)	−0.00698 (3)	C50	0.1410 (3)	0.6883 (3)	0.4141 (4)
M2	0.17409 (2)	0.33936 (2)	−0.04127 (3)	C51	0.1232 (3)	0.5697 (3)	0.3551 (5)
M3	0.24524 (3)	0.27815 (3)	0.22493 (4)	C52	0.2581 (3)	0.8704 (3)	0.5488 (4)
M4	0.12838 (4)	0.11868 (4)	−0.14643 (5)	C53	0.3681 (4)	0.9513 (3)	0.6385 (5)
				C54	0.3491 (3)	0.7654 (3)	0.3977 (4)
O11	0.5443 (2)	0.4458 (2)	0.1699 (3)	C55	0.3290 (3)	0.8208 (3)	0.2646 (4)
O12	0.4380 (3)	0.0664 (3)	0.0672 (5)	C56	0.3027 (3)	0.6997 (3)	0.6220 (4)
O13	0.4131 (3)	0.2874 (3)	−0.2968 (3)	C57	0.2297 (4)	0.6827 (3)	0.7348(5)
O21	0.3182 (3)	0.5748 (2)	0.0903 (3)				
O22	−0.0567 (2)	0.3547 (2)	0.0007 (4)	H50A	0.1200 (0)	0.7255 (0)	0.3337 (0)
O23	0.1705 (3)	0.3896 (2)	−0.3489 (3)	H50B	0.0891 (0)	0.6879 (3)	0.4781 (0)
O31	0.0370 (2)	0.2516 (3)	0.3533 (3)	H52A	0.2006 (0)	0.8606 (0)	0.6063 (0)
O32	0.3575 (2)	0.1359 (2)	0.3951 (3)	H52B	0.2344 (0)	0.9035 (0)	0.4655 (0)
O33	0.3862 (2)	0.4975 (2)	0.4135 (3)	H54A	0.3505 (0)	0.6920 (0)	0.3661 (0)
O41	−0.1279 (2)	0.0480 (2)	−0.2152 (3)	H54B	0.4253 (0)	0.8072 (0)	0.4538 (0)
O42	0.1575 (3)	−0.1018 (3)	−0.1026 (4)	H56A	0.3804 (0)	0.7443 (0)	0.6703 (0)
O43	0.1447 (3)	0.1013 (3)	−0.4586 (3)	H56B	0.3061 (0)	0.6281 (0)	0.5847 (0)
				H51A	0.1660 (0)	0.5625 (0)	0.2773 (0)
N	0.1823 (2)	0.1959 (2)	0.0395 (3)	H51B	0.0423 (0)	0.5316 (0)	0.3148 (0)
N2	0.2631 (2)	0.7557 (2)	0.4956 (3)	H51C	0.1465 (0)	0.5319 (0)	0.4323 (0)
C11	0.4677 (3)	0.3748 (3)	0.1041 (4)	H53A	0.3613 (0)	1.0215 (0)	0.6680 (0)
C12	0.4052 (3)	0.1378 (3)	0.0395 (4)	H53B	0.4276 (0)	0.9649 (0)	0.5815 (0)
C13	0.3857 (3)	0.2745 (3)	−0.1889 (4)	H53C	0.3940 (0)	0.9217 (0)	0.7222 (0)
C21	0.2640 (3)	0.4851 (3)	0.0433 (4)	H55A	0.3320 (0)	0.8945 (0)	0.2773 (0)
C22	0.0286 (3)	0.3463 (3)	−0.0165 (4)	H55B	0.2533 (0)	0.7799 (0)	0.2090 (0)
C23	0.1700 (3)	0.3667 (3)	−0.2337 (4)	H55C	0.3836 (0)	0.8171 (0)	0.2068 (0)
C31	0.1166 (3)	0.2624 (3)	0.3083 (4)	H57A	0.1406 (0)	0.6250 (0)	0.6953 (0)
C32	0.3128 (3)	0.1904 (3)	0.3347 (4)	H57B	0.2243 (0)	0.7523 (0)	0.7707 (0)
C33	0.3351 (0)	0.4140 (3)	0.3448 (4)	H57C	0.2639 (0)	0.6525 (0)	0.8141 (0)
C41	−0.0298 (3)	0.0743 (3)	−0.1871 (4)				
C42	0.1449 (3)	−0.0184 (3)	0.1214 (4)				
C43	0.1384 (3)	0.1100 (3)	−0.3403 (4)				

Table VIII. Bond Distances (Å) for $Et_4N[FeRu_3N(CO)_{12}]$

M1–M2	2.650 (1)	C11–O11	1.136 (4)
M1–M3	2.739 (1)	C12–O12	1.133 (5)
M1–M4	2.740 (1)	C13–O13	1.139 (4)
M2–M3	2.763 (1)	C21–O21	1.139 (4)
M2–M4	2.750 (1)	C22–O22	1.138 (4)
M3–M4	3.717 (1)	C23–O23	1.147 (4)
		C31–O31	1.121 (4)
N–M1	2.067 (2)	C32–O32	1.139 (4)
N–M2	2.051 (2)	C33–O33	1.135 (4)
N–M3	1.872 (2)	C41–O41	1.140 (4)
N–M4	1.846 (2)	C42–O42	1.139 (4)
		C43–O43	1.132 (4)
M1–C11	1.890 (4)		
M1–C12	1.893 (4)	N2–C50	1.527 (4)
M1–C13	1.892 (4)	N2–C52	1.526 (4)
M2–C21	1.874 (3)	N2–C54	1.518 (4)
M2–C22	1.896 (4)	N2–C56	1.519 (4)
M2–C23	1.870 (4)		
M3–C31	1.872 (4)	C50–C51	1.501 (5)
M3–C32	1.862 (3)	C52–C53	1.501 (5)
M3–C33	1.893 (4)	C54–C55	1.506 (5)
M4–C41	1.836 (4)	C56–C57	1.506 (5)
M4–C42	1.841 (4)		
M4–C43	1.853 (4)		

The final refinement shows that the iron is not randomly disordered throughout the cluster and the best model contained 74% iron in the wing-tip positions and 26% iron in the hinge positions.

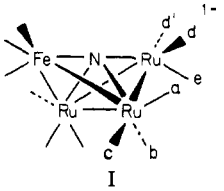

I

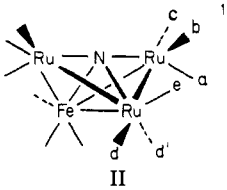

II

A kinetic study of reaction 11 was undertaken. The progress of the reaction was monitored for 2 half-lives by observation of the intensity of the bridging carbonyl stretching frequency at 1823 cm^{-1}. Longer times were prevented from analysis because of the small amounts of $[FeRu_4N(CO)_{14}]^-$ that began to form. Figure 2 shows a typical plot of the ln $[FeRu_3(CO)_{12}(NO)]^-$ vs. time, and these data indicate the reaction is first order in cluster concentration. Analysis of the CO dependence of the rate was prohibited because of cluster degradation (reaction 9).

The reaction was also monitored by ^{13}C NMR spectroscopy. As stated above, $[FeRu_3N(CO)_{12}]^-$ exists in two isomeric forms in the solid state. Infrared and ^{13}C and ^{15}N NMR spectroscopic studies clearly show that both of these isomers exist in solution, and the details of the assignments of the structures and the isomerization process are discussed below. When the NMR tube containing ^{13}C-enriched $PPN[FeRu_3(CO)_{12}(NO)]$ was heated to 67 °C for 30 min the $[FeRu_3N(CO)_{12}]^-$ that formed was not present at the equilibrium ratio of I/II. Rather, the ratio of Fe (wing-tip) to Fe (hinge) was 2.1:1. At this temperature a correction for the amount of direct isomerization of the two isomers would be small in 30 min and would slightly decrease the above ratio.

Formation of $[FeRu_4N(CO)_{14}]^-$. Extended pyrolysis of $[FeRu_3N(CO)_{12}]^-$ produced small quantities of a new cluster that we have identified as $[FeRu_4N(CO)_{14}]^-$. A more efficient preparation involves the direct condensation of $[FeRu_3N(CO)_{12}]^-$ with $Ru_3(CO)_{12}$ in refluxing THF for 50 h. The formulation was based on elemental analysis and the FAB mass spectral data that indicated an intense parent ion for the cluster. The infrared spectrum showed the presence of both bridging and terminal carbonyls, and the ^{13}C NMR spectrum exhibited two resonances at 204.5 and 213.2 ppm with relative intensities of 11:3, respectively. The structure of this cluster is probably the same as the square-pyramidal nitrido cluster $[Ru_5N(CO)_{14}]^-$.[14] Since the ^{13}C resonance of intensity 3 is located in the iron carbonyl region, we suggest that the iron is in the apical position. This is based on the similarity of the spectrum with that reported for $[Fe_5N(CO)_{14}]^-$.[7]

Solution Structures of $[FeRu_3N(CO)_{12}]^-$. Experiments described in this section will be broken into four groups. First, we will address the assignment of the spectroscopic data to the two

Table IX. Selected Bond Angles (deg) for $Et_4N[FeRu_3N(CO)_{12}]$

M2–M1–M3	61.67 (1)	M4–M2–N	42.17 (2)
M2–M1–M4	61.33 (1)	M1–M3–M2	57.58 (1)
M2–M1–N	49.68 (6)	M1–M3–N	48.95 (7)
M2–M1–C11	101.6 (1)	M1–M3–C31	152.0 (1)
M2–M1–C12	151.7 (1)	M1–M3–C32	95.0 (1)
M2–M1–C13	98.1 (1)	M1–M3–C33	108.8 (1)
M3–M1–M4	85.44 (1)	M2–M3–N	47.92 (7)
M3–M1–N	43.09 (7)	M2–M3–C31	101.8 (1)
M3–M1–C11	82.7 (1)	M2–M3–C32	150.1 (1)
M3–M1–C12	101.4 (1)	M2–M3–C33	105.0 (1)
M3–M1–C13	158.9 (1)	N–M3–C31	103.5 (1)
M4–M1–N	42.35 (7)	N–M3–C32	106.2 (1)
M4–M1–C11	162.5 (1)	N–M3–C33	149.9 (1)
M4–M1–C12	96.8 (1)	C31–M3–C32	99.0 (2)
M4–M1–C13	89.9 (1)	C21–M3–C33	94.2 (2)
N–M1–C11	124.6 (1)	C32–M3–C33	94.6 (1)
N–M1–C12	102.2 (2)	M1–M4–M2	57.72 (1)
N–M1–C13	129.1 (1)	M1–M4–N	48.95 (7)
C11–M1–C12	98.0 (2)	M1–M4–C41	154.4 (1)
C11–M1–C13	96.7 (2)	M1–M4–C42	99.2 (1)
C12–M1–C13	99.6 (2)	M1–M4–M43	103.0 (1)
M1–M2–M3	60.75 (1)	M2–M4–N	48.23 (7)
M1–M2–M4	60.95 (1)	M2–M4–C41	99.0 (1)
M1–M2–N	50.21 (7)	M2–M4–C42	149.8 (1)
M3–M2–M4	84.78 (1)	M2–M4–C43	108.0 (1)
M3–M2–N	42.65 (7)	N–M4–C41	108.7 (1)
N–M4–C42	102.5 (1)	M3–C31–O31	177.5 (3)
N–M4–C43	148.5 (1)	M3–C32–O32	175.8 (3)
C41–M4–C42	98.0 (2)	M3–C33–O33	177.1 (3)
C41–M4–C43	94.0 (2)	M4–C41–O41	178.4 (3)
C42–M4–C43	95.4 (2)	M4–C42–O42	178.1 (3)
M1–N–M2	80.11 (8)	M4–C43–O43	177.8 (4)
M1–N–M3	88.0 (1)	C50–N2–C52	105.8 (2)
M1–N–M4	88.7 (1)	C50–N2–C54	111.4 (2)
M2–N–M3	89.4 (1)	C50–N2–C56	111.1 (3)
M2–N–M4	89.6 (1)	C52–N2–C54	111.1 (3)
M3–N–M4	176.6 (2)	C52–N2–C56	111.2 (2)
M1–C11–O11	177.7 (3)	C54–N2–C56	106.4 (2)
M1–C12–O12	177.8 (4)	N2–C50–C51	115.7 (3)
M1–C13–O13	178.4 (3)	N2–C52–C53	115.9 (3)
M2–C21–O21	177.8 (3)	N2–C54–C55	116.4 (3)
M2–C22–O22	177.3 (3)	N2–C56–C57	115.5 (3)
M2–C23–O23	176.2 (3)		

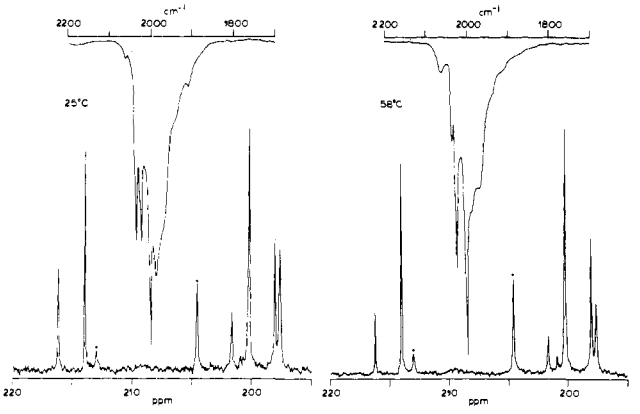

Figure 7. Comparison of the ^{13}C NMR and infrared spectra of $[FeRu_3N(CO)_{12}]^-$ equilibrated at 25 and 58 °C. The marked (+) peaks are due to the impurity $[FeRu_4N(CO)_{14}]^-$.

structures I and II. We will follow this with an examination of the low-temperature ^{13}C NMR data that allows us to probe the fluxional processes for CO interconversions. Next, the data will be presented that allows the derivation of the thermodynamic parameters for the equilibrium between the isomers, and finally, we will describe the experiment that gives the rate of isomerization at one temperature.

Figure 7 shows a comparison of the ^{13}C NMR and IR spectra of equilibrated mixtures of $[FeRu_3N(CO)_{12}]^-$ at two different temperatures. These data allow us to correlate the ν_{CO} absorbance at 2036 cm^{-1} with the ^{13}C resonances at 216.3, 201.7, and 197.6

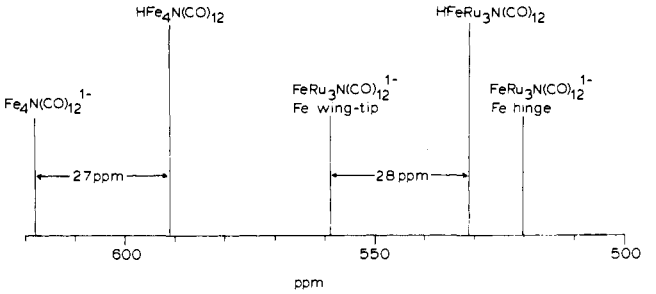

Figure 8. Effect of protonation on the ^{15}N chemical shift of related nitrido clusters.

ppm (spectral set B) and the ν_{CO} peak at 2023 cm^{-1} with the ^{13}C resonances at 214.0, 200.2, and 198.1 ppm (spectral set A). In both isomers the iron carbonyl resonances are downfield from the ruthenium carbonyl resonances. The above information does not allow us to assign one isomer to one set of spectra. Three independent arguments support the assignment of I to the spectral set A and II to set B. First, the results from the single-crystal X-ray crystallographic analysis distinctly show that iron is preferentially located in the wing-tip position (I). From this we conclude that isomer I, which is the predominant species in solution under all conditions studied, can be assigned to spectral set A. We are aware that the process of crystallization could favor one isomer over the other, but our assignment does not rest entirely on this result.

The ^{15}N NMR data are also useful in assigning the geometry of the cluster. The two isomers have chemical shifts that differ by 39 ppm (I, 559 ppm; II, 520 ppm) (Figure 8). The protonated molecule $HFeRu_3N(CO)_{12}$, which has the Fe in the wing-tip position, exhibits one resonance at 531 ppm. The effect of protonation on the ^{15}N chemical shift of $[Fe_4N(CO)_{12}]^-$ (618 ppm) causes a 27 ppm upfield shift to 591 ppm for $HFe_4N(CO)_{12}$. For $[FeRu_3N(CO)_{12}]^-$ there is an essentially identical upfield shift (28 ppm) in going from the isomer giving rise to the resonance at 559 ppm to $HFeRu_3N(CO)_{12}$. Once again this result suggest that iron is in the wing-tip position in the more abundant isomer (559 ppm).

Finally, the structure of $HFeRu_3N(CO)_{12}$, which will be discussed in detail in a separate paper, has the $Fe(CO)_3$ exclusively in the wing-tip position. The hydrogen, which bridges the hinge Ru–Ru bond, can be removed (at room temperature) by using KH. When the deprotonation is monitored by infrared spectroscopy, we see the formation of one isomer, that having absorbances assigned to I. The implication is that the anion has the same metal arrangement as its conjugate acid. The combination of these three arguments provides convincing evidence of the solution structures of the isomers I and II.

A trend that may be useful in future structural assignments is revealed by careful examination of the ^{13}C resonances. In all cases for $[FeRu_3N(CO)_{12}]^-$ the average chemical shift of the three carbonyls in $M(CO)_3$ groups of the wing-tip sites are ~2–4 ppm upfield of the resonances for the hinge positions.

The fluxional properties of $[FeRu_3N(CO)_{12}]^-$ were studied by using a sample that was equilibrated at 35 °C to bring the ratio of I/II to 2.4:1. This gave a reasonable concentration of both isomers while allowing a clear distinction to be made between the peaks due to isomer I and those due to isomer II. Each isomer was expected to give a 2:2:2:2:1 pattern for the ruthenium carbonyls in the low-temperature limiting spectrum. By using the 2.4 ratio of I/II, all the carbonyl peaks for I were bigger than all the peaks for II in the slow-exchange spectrum. The exchange process is a spinning of the metal tricarbonyl groups so that a, b, and c become equivalent in the fast exchange limit, as do d and e.

At −100 °C the resonances for the two iron tricarbonyl groups are still singlets, although slightly broadened. All ten peaks from the ruthenium carbonyls are clearly resolved and consist of five larger peaks from isomer I in the expected 2:2:2:2:1 pattern, as well as five smaller peaks from isomer II, also in the same pattern.

We will consider isomers I and II separately.

At −100 °C the motion exchanging the ruthenium carbonyls of I is completely frozen out. The peak of height one at δ 203.7 can logically be assigned to carbonyl e. As the temperature is raised to −90 °C, the peaks at δ 189.8, 204.8, and 205.3 broaden simultaneously and the remainder of the spectrum is unchanged, suggesting that these three peaks are due to carbonyls a, b and c that are exchanging with each other. By −65 °C the peaks at δ 194.6 and 203.7 due to wing-tip carbonyls d and e are significantly broadened. Since e is exchanging with d every time the tricarbonyl group spins and d exchanges with e only every other time, e is collapsing faster than d. At −25 °C the peak due to the hinge ruthenium carbonyl set is beginning to grow back in, and by −5 °C all peaks are again visible. At 25 °C three sharp peaks are observed at δ 214.0 (Fe), 200.2 (a, b, c), and 198.1 (d, e).

As with isomer I the motion exchanging the ruthenium carbonyls in II is completely frozen out at −100 °C. The peak of height one at δ 192.9 is due to the unique carbonyl e, bound to the hinge ruthenium atom. When the temperature is raised to −80 °C, the peaks at δ 192.9 and 205.8 begin to broaden, the former broadening slightly faster than the latter. This is consistent with the peak at 205.8 ppm belonging to the carbonyls labeled d. By −65 °C the peaks at δ 193.3, 194.2, and 203.3 are broadened and can be assigned to the wing-tip carbonyls a, b, and c. From this temperature up to 25 °C the dynamics are similar to isomer I. At 25 °C three sharp peaks are observed at δ 216.2 (Fe), 197.6 (a, b, c), and 201.8 (d, e) in the fast-exchange limiting spectrum.

The equilibrium between the isomers of $[FeRu_3N(CO)_{12}]^-$ was measured over the temperature range from 25 to 68 °C. One solution of the cluster was divided into six NMR tubes that were sealed and brought to the appropriate temperature. The ^{13}C NMR spectrum was periodically measured until no further change in the intensities was observed, and then with the total integrated intensity for all of the carbonyl resonances of each isomer, the values listed in Table II were obtained. The ΔH and ΔS for the reaction of I ⇄ II are −3.5 ± 1.0 kcal/mol and −13 ± 2 eu.

The rate at which equilibrium was reached was also studied by using ^{13}C NMR spectroscopy. A sample of ^{13}CO-enriched $HFeRu_3N(CO)_{12}$ was prepared and subsequently deprotonated by using KH in THF. As previously stated the iron is located exclusively in the wing-tip position in $HFeRu_3N(CO)_{12}$. At room temperature this reaction is complete overnight and results in the formation of the isomer of $[FeRu_3N(CO)_{12}]^-$ with the Fe in the wing-tip position. The sample was dissolved in THF and sealed in a NMR tube and maintained at 27 °C for 10 days until equilibrium was reached. Figure 4 shows a plot of ln $(\chi_{II}(eq) - \chi_{II}(t))$ vs. time which yields a value of $(4.2 \pm 0.2) \times 10^{-7}$ s^{-1} for k_f.

Discussion

Formation of $[FeRu_3(CO)_{12}(NO)]^-$. No intermediates are observed in the reaction of $[Fe(CO)_3(NO)]^-$ with $Fe_3(CO)_{12}$ to generate the nitrido cluster $[Fe_4N(CO)_{12}]^-$.[11,12] Although the same is true for the reaction of $[Ru(CO)_3(NO)]^-$ with $Ru_3(CO)_{12}$ to form $[Ru_4N(CO)_{12}]^-$,[31] we have isolated the intermediate in the cross reaction of $[Fe(CO)_3(NO)]^-$ with $Ru_3(CO)_{12}$. A preliminary kinetic study of the reaction was undertaken for two reasons. First, we needed to optimize the conditions to produce high yields of $[FeRu_3(CO)_{12}(NO)]^-$. Second, although the redox condensation has been extensively used in cluster syntheses, no kinetic studies have been reported. The results clearly indicate that the reaction is independent of the concentration of $[Fe(CO)_3(NO)]^-$ and is inhibited by the presence of CO. From this we infer that the initial step is CO dissociation from $Ru_3(CO)_{12}$ to give the unsaturated cluster $Ru_3(CO)_{11}$. This species should readily react with $[Fe(CO)_3(NO)]^-$ to form $[FeRu_3(CO)_{14}(NO)]^-$; however, no intermediates can be spectroscopically observed in the overall reaction. This implies that the further loss of two CO's from $[FeRu_3(CO)_{14}(NO)]^-$ occurs rapidly to generate the final product. We note the similarity of this reaction with reaction 12, where neither the intermediate mono- nor disubstituted cluster can be isolated.[32]

$$Ru_3(CO)_{12} + 3PPh_3 \rightarrow Ru_3(CO)_9(PPh_3)_3 + 3CO \quad (12)$$

The molecular structure of the anion $[FeRu_3(CO)_{12}(NO)]^-$ is nearly identical with the isoelectronic cluster $[CoRu_3(CO)_{13}]^-$.[33] However, the crystal structure is different. $PPN[CoRu_3(CO)_{13}]$ crystallizes in the space group $P\bar{1}$ whereas $PPN[FeRu_3(CO)_{12}(NO)]$ forms crystals in $P2_1/c$. The major difference between the compounds is in the P–N–P angle of the cation. For the cobalt structure this value is 140.0 (2)°, which is consistent with the vast majority of the PPN^+ salts. For the iron nitrosyl analogue the value is 168.9 (3)° and is unique.[28,30]

Formation and Structure of $[FeRu_3N(CO)_{12}]^-$. The nitrosyl cluster $[FeRu_3(CO)_{12}(NO)]^-$ reacts releasing CO_2 and forming the nitrido cluster $[FeRu_3N(CO)_{12}]^-$. For practical purposes the nitrido cluster can be directly formed from $[Fe(CO)_3(NO)]^-$ and $Ru_3(CO)_{12}$ in 73% yield. Although the overall structure is similar to other butterfly clusters containing interstitial atoms, the remarkable feature of the analysis is the determination that both isomers (I + II) have cocrystallized. The experimentally determined ratio of isomer I (with Fe in the wing-tip position) to isomer II (with Fe in the hinge position) is 3.0. This value was derived by refining the multiplicities of the ruthenium atoms in each site of the cluster for the Et_4N^+ salt.

The studies of $[FeRu_3N(CO)_{12}]^-$ in solution are in complete accord with the solid-state structure. The assignment of the IR, ^{15}N NMR, and ^{13}C NMR spectra to the various isomers is based on three arguments, which have been detailed in the Results. In the following discussion we will consider the dynamic processes that are responsible for the averaging of the carbonyls and the interconversion of the two isomers. The ^{13}C NMR spectra of $[FeRu_3N(CO)_{12}]^-$ in the temperature range of −100 to +25 °C indicate that the only process occurring is localized CO exchange on the individual metals. Even at −100 °C the iron carbonyls are still rapidly interconverting in both isomers; however, the rearrangements of the $Ru(CO)_3$ groups have been slowed so that they exhibit their low-temperature limiting spectrum. As the temperature is raised, two simple processes occur nearly simultaneously in both isomers. First, the carbonyls begin to spin around the hinge ruthenium positions (coalescence temperature ≈ −80 °C). Second, the same process begins to occur on the wing-tip ruthenium atoms at −65 °C. No further averaging occurs, and by +25 °C sharp average resonances are observed for the six different metal sites in the two isomers. The CO scrambling mechanism observed here is the same as that reported for $HFe_4(CH)(CO)_{12}$, III.[34] One

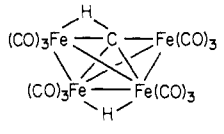

III

important difference that exists in III is that the barrier for CO scrambling on the wing-tip positions is less than that for the hinge metals. The probable cause of this difference is the presence of the hydrogen bridging the hinge Fe–Fe bond. In a recent study[35] of $[Os_3(CO)_{10}(NO)]^-$, IV, the CO scrambling on the $Os(CO)_3$ groups was found to occur at much lower temperature than on the $Os(CO)_4$ group. In the previously studied[36] protonated

(31) Gladfelter, W. L.; Stevens, R. E.; Fjare, D. E. "3rd International Symposium on Homogeneous Catalysis", Milano, Italy, Aug 1982, Abstract Tu5.

(32) Malik, S. K.; Poë, A. *Inorg. Chem.* **1978**, *17*, 1484.

(33) Steinhardt, P. C.; Gladfelter, W. L.; Harley, A. D.; Fox, J. R.; Geoffroy, G. L. *Inorg. Chem.* **1980**, *19*, 332.

(34) Beno, M. A.; Williams, J. M.; Tachikawa, M.; Muetterties, E. L. *J. Am. Chem. Soc.* **1981**, *103*, 1485.

(35) Johnson, B. F. G.; Lewis, J.; Mace, J.; Raithby, P. R.; Stevens, R. E.; Gladfelter, W. L. *Inorg. Chem.* **1984**, *23*, 1600.

(36) Bryan, E. G.; Forster, A.; Johnson, B. F. G.; Lewis, J.; Matheson, T. W. *J. Chem. Soc., Dalton Trans.* **1978**, 196.

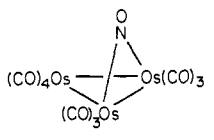

IV

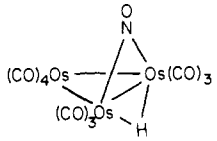

V

analogue V, the $Os(CO)_3$ groups remained static even at high temperature while the carbonyls on the $Os(CO)_4$ were undergoing rapid interconversion. The inversion of the activation parameters of the two sites was attributed to the bridging hydrogen atom.

The direct interconversion of the two isomers I and II is not detectable on the ^{13}C NMR time scale even at elevated temperatures. The first evidence suggesting that this was occurring came from infrared spectroscopy. Refluxing a solution of $[FeRu_3N(CO)_{12}]^-$ in THF caused a major change of the relative intensities of the absorbances in the carbonyl region. When the solution was cooled to room temperature, the process slowly (~8 days) reversed itself. This cycle was repeated several times with no loss of material.

The inherent difficulties in extracting the concentration of the isomers from the infrared data prompted us to turn to another technique, ^{13}C NMR spectroscopy, to analyze the equilibrium. By comparison of the total intensities of the carbonyl absorbances of both isomers obtained in the temperature range from 25 to 68 °C in THF, we derived the thermodynamic values of $\Delta H = -3.5 \pm 1.0$ kcal/mol and $\Delta S = -13 \pm 2$ eu for I $\rightleftarrows$ II. The difference in enthalpic content of the two isomers is significant but still small enough to say that there is no outstanding energetic reason for locating the iron in the hinge vs. the wing-tip position. On the other hand, the entropic differences between the two isomers is large and cannot be easily reconciled merely on the basis of their structures. At this point it is helpful to recall that the cluster is anionic and that the solution also contains the PPN cation. Differences in the nature and/or the extent of ion pairing of the PPN cation with the two isomeric anions may be responsible for the large ΔS observed. Darensbourg and co-workers[37] have extensively studied the ion pairs formed in aprotic solutions of PPN^+ salts of carbonylmetalates. For instance, the dissociation constant for the ion pair between PPN^+ and $[Co(CO)_4]^-$ is 9.4×10^{-5} in THF at 22 °C. Since the negative charge is more delocalized in $[FeRu_3N(CO)_{12}]^-$, the corresponding value would be expected to be increased. Is there any reason to suggest that a difference in ion pairing of the two isomers is reasonable? Such a difference would have to be related to a difference in the charge distribution in the two isomers. Since protonation of $M_4X(CO)_{12}^{y-}$ butterfly clusters leads to the hydrogen bridging of the hinge M–M bond, it is reasonable to suggest that this is the location of the charge in the anion. Since iron is slightly more electronegative than ruthenium, placing the iron in the hinge position would tend to localize more charge on the iron and create a charge difference between the two hinge metal atoms. When iron is in the wing-tip position, the negative charge is equally distributed on the two hinge ruthenium atoms. Examination of the infrared spectrum offers some support for this argument. When iron is in the hinge position (II), the lowest energy ν_{CO}, which to some extent indicates the amount of negative charge delocalized onto the ligands, is at 1909 cm^{-1} compared to 1950 cm^{-1} for the other isomer. Consistent with this argument, the highest energy intense peak for II is 2035 cm^{-1} compared to 2020 cm^{-1} for I.

At 27 °C the rate of conversion of I to II is $(4.2 \pm 0.2) \times 10^{-7}$ s^{-1} and is not retarded by CO. Two possible mechanisms for the rearrangement are illustrated in Scheme I. The first involves a pairwise exchange of the metal through a square-pyramidal intermediate and is analogous to the Berry pseudorotation. The second mechanism involves a trigonal-bipyramidal intermediate and does not involve pairwise metal site exchange. For $[FeRu_3N(CO)_{12}]^-$ neither one of these mechanisms can be eliminated.

Scheme I

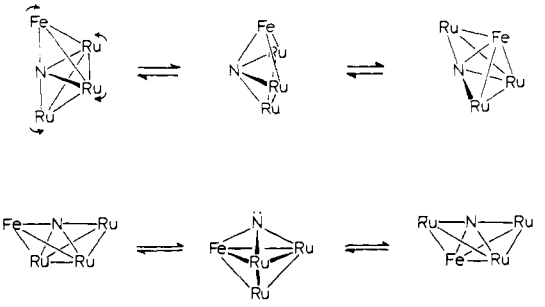

However, the fact that structures related to the trigondal-bipyramidal intermediate such as $Os_4(CO)_{12}NMe$, VI, are known[38]

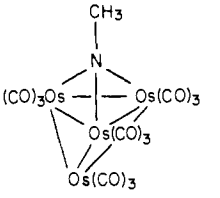

VI

suggest that it may have a lower activation barrier. Intermolecular mechanisms can be ruled out since we observe no $[Fe_4N(CO)_{12}]^-$, $[Ru_4N(CO)_{12}]^-$, or $[FeRu_4N(CO)_{14}]^-$ formation in the course of several cycles of the experiment. If mononuclear metal carbonyl fragments were liberated, these stable products, which would result from scrambling of the metals, would be observable.

Mechanism of the NO Deoxygenation. From the studies of $[FeRu_3(CO)_{12}(NO)]^-$ we know that the deoxygenation (a) is first order in the cluster concentration, (b) generates the nitrido cluster in a 2:1 isomer ratio of I (Fe = wing-tip) to II (Fe = hinge), and (c) is probably intramolecular. This last point is based on the lack of observation of scrambling of the metals in the reaction. This particular reaction, while being less complex than reaction 4, still must involve several steps. Even an understanding of the first step is made difficult, since the test for CO inhibition cannot be conclusive. The activation parameters obtained are consistent with a unimolecular process such as metal–metal bond cleavage or CO dissociation. Attempts to trap intermediates with $P(OCH_3)_3$ also resulted in disruption of $[FeRu_3(CO)_{12}(NO)]^-$ and were of no mechanistic value. The origin of the 2:1 isomer ratio must arise when the M–M bond is cleaved. Simple geometric considerations of the tetrahedral $FeRu_3$ core suggest that if a ligand bridging an $FeRu_2$ face were able to randomly insert into any of the adjacent M–M bonds, it would generate a product mixture where the Fe–Ru bond cleavage product was formed twice as often as the Ru–Ru bond cleavage product. Such an argument requires that the transition-state energies for the paths are similar. This is possible if the reaction is reasonably exothermic and the transition states are energetically close to the starting material. Scheme II summarizes some of the possible steps for the deoxygenation of the NO. In path A a simple rearrangement converting the terminal nitrosyl to a triply bridging NO could generate VII having a three fold symmetry axis (ignoring the differences in the metals). Such a structure can be considered as a trigonal-bipyramidal cluster with the NO occupying an axial site. An isomerization to VIII with NO now in an equatorial site would involve M–M bond cleavage. Since the μ-NO is bridging an $FeRu_2$ face, this is a reasonable step to explain the product selectivity. This cluster could proceed to the product by complete N–O dissociation to a nitride and oxide ligand (CO loss would be required) or by direct oxygen atom transfer to a coordinated CO. Alternatively, in path B initial CO loss could induce the NO to bind as an η-NO that would now donate five electrons to the cluster. Metal–metal bond cleavage would require an additional two electrons to be

(37) Darensbourg, M.; Barros, H.; Borman, C. *J. Am. Chem. Soc.* **1977**, *99*, 1647.

(38) Lin, Y. C.; Knobler, C. B.; Kaesz, H. D. *J. Organomet. Chem.* **1981**, *213*, C41.

Scheme II

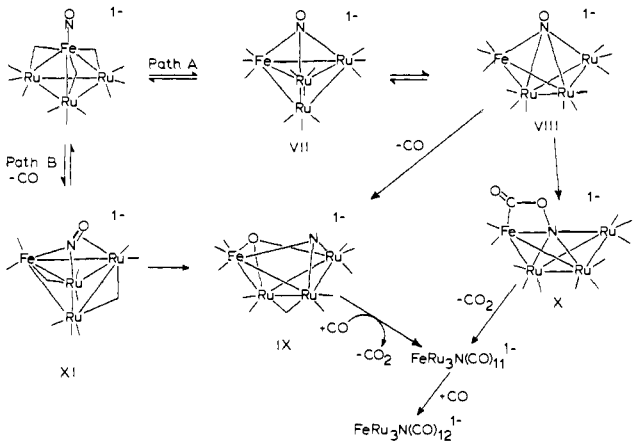

donated to the cluster and could result in the N–O bond cleavage.

Conclusions

In this study we have evaluated the conversion of a nitrosyl ligand to a nitrido ligand on a tetranuclear cluster. The data suggest that the conversion is intramolecular and possible mechanistic pathways have been suggested. The butterfly cluster $[FeRu_3N(CO)_{12}]^-$ exists in two isomeric forms both in the solid state and in solution. The thermodynamic and kinetic parameters for the interconversion of the isomeric forms provide the first evidence that the wing-tip and hinge positions of butterfly clusters having μ_4-bridging atoms can interconvert.

The isolation of $[FeRu_3(CO)_{12}(NO)]^-$ has afforded us a unique opportunity to study in detail a complex and important reaction of a metal cluster. Studies such as this provide strong evidence supporting the idea that multiple coordination sites are valuable for activating small molecules. Further work in progress is designed toward the synthesis of new molecules that may allow us to directly observe some of the suggested reaction intermediates in Scheme II.

Acknowledgment. We wish to thank the National Science Foundation for supporting this research (Grant No. CHE-8106096) and Doyle Britton and Robert Stevens for valuable assistance with the x-ray diffraction studies. The FAB mass spectrum was obtained from the Midwest Center for Mass Spectrometry at the University of Nebraska.

Registry No. I, 90968-63-1; I·Et_4N, 90968-65-3; I·PPN, 90968-68-6; II, 90968-66-4; II·Et_4N, 90968-67-5; II·PPN, 90968-69-7; PPN[$FeRu_3(CO)_{12}(NO)$], 76791-97-4; PPN[$FeRu_4N(CO)_{14}$], 90990-44-6; PPN[$Fe(CO)_3(NO)$], 61003-17-6; $Et_4N[Fe(CO)_3(NO)]$, 35610-51-6; $[Fe(CO)_3(NO)]^-$, 15020-24-3; $Ru_3(CO)_{12}$, 15243-33-1; $P(OCH_3)_3$, 121-45-9.

Supplementary Material Available: A listing of the rate data for reaction 11 and the isomerization of I to II as well as the details of the crystallographic studies (37 pages). Ordering information is given on any current masthead page.

Coordination Chemistry of Pyridines on Ni(100)

R. M. Wexler* and E. L. Muetterties†

Contribution from the Materials and Molecular Research Division, Lawrence Berkeley Laboratory, and the Department of Chemistry, University of California, Berkeley, California 94720. *Received December 19, 1983*

Abstract: The coordination chemistry of methyl-substituted pyridine molecules on Ni(100) is described. The position of methyl substitution had a profound effect upon pyridine surface chemistry. 4-Methylpyridine behaved analogously to pyridine and showed extensive molecular desorption. The decomposition of this pyridine yielded H_2 in three different maxima: the data suggest that the first step yields α-pyridyl and that the CH_3 C–H bonds are not cleaved at low temperatures (as is the case for 3,5-dimethylpyridine). In contrast, both 2-methylpyridine and 2,6-dimethylpyridine show CH_3 C–H bond breaking at low temperatures. These results are discussed in terms of the C_5N ring orientation with respect to the Ni(100) plane for this methylpyridine chemistry.

We have previously reported[1] on the chemistry of pyridine on nickel surfaces. Through the use of specific isotope labeling, the reversible regiospecific scission of α carbon–hydrogen bonds was demonstrated for pyridine coordinated to Ni(100). However, no information about the coordination geometry of the pyridine molecule was obtained. The issue of pyridine coordination to transition-metal surfaces has been a subject of controversy with respect to the disposition of the pyridine ring relative to the surface and the primary mode of interaction. Pyridine is believed to bind to Pt(111) and -(100)[2] through the nitrogen atom on the basis of work function measurements. Near-edge X-ray absorption studies[3] have established chemisorbed pyridine on Pt(111) to be perpendicular to the surface plane, at least for coverages above ~0.1 monolayer. However, recent photoemission data indicate that either or both the nitrogen lone pair and the aromatic electrons may be involved in the bonding of pyridine to Pd(111),[4a] Ir(111),[4b] Cu(110),[5] and Ag(111).[6] Described below are thermal desorption studies of methyl-substituted pyridines on Ni(100). The variation in the hydrogen desorption due to decomposition of the methyl substituent appears to provide insight to the orientation of the ring with respect to the surface and also to the molecular motion which

* Present address: Department of Chemistry 127-72, California Institute of Technology, Pasadena, CA 91125.
† Deceased January 12, 1984.

(1) Wexler, R. M.; Tsai, M.-C.; Friend, C. M.; Muetterties, E. L. *J. Am. Chem. Soc.* **1982**, *104*, 2034.
(2) Gland, J. L.; Somorjai, G. A. *Surf. Sci.* **1973**, *38*, 157; *Adv. Coll. Interface Sci.* **1976**, *5*, 205.
(3) Johnson, A. J.; Muetterties, E. L.; Stöhr, J. *J. Am. Chem. Soc.* **1983**, *105*, 7183.
(4) (a) Netzer, F. P.; Mack, J. U. *Chem. Phys. Lett.* **1983**, *95*, 492; *J. Chem. Phys.* **1983**, *79*, 1017.
(5) Bandy, B. J.; Lloyd, D. R.; Richardson, N. V. *Surf. Sci.* **1979**, *89*, 344.
(6) Demuth, J. E.; Christmann, K.; Sanda, P. N. *Chem. Phys. Lett.* **1980**, *76*, 201.

0002-7863/84/1506-4810$01.50/0